AD-A099 360 WISCONSIN UNIV-MADISON MATHEMATICS RESEARCH CENTER F/G 12/1
THE BIFURCATION BEHAVIOR OF TUBULAR REACTORS.(U)
JAN 81 K F JENSEN, W H RAY DAAG29-80-C-0041
UNCLASSIFIED MRC-TSR-2172 NL

1 OF 1
AD A099360

END
DATE FILMED
DTIC

MRC Technical Summary Rep... 72

THE BIFURCATION BEHAVIOR OF TUBULAR REACTORS

Klavs F. Jensen and W. Harmon Ray

Mathematics Research Center
University of Wisconsin—Madison
610 Walnut Street
Madison, Wisconsin 53706

January 1981

Received December 5, 1980

Approved for public release
Distribution unlimited

Sponsored by

U. S. Army Research Office
P.O. Box 12211
Research Triangle Park
North Carolina 27709

National Science Foundation
Washington, D. C. 20550

UNIVERSITY OF WISCONSIN - MADISON
MATHEMATICS RESEARCH CENTER

THE BIFURCATION BEHAVIOR OF TUBULAR REACTORS

Klavs F. Jensen[†] and W. Harmon Ray[*]

Technical Summary Report #2172

ABSTRACT

Methods for studying the bifurcation behavior of tubular reactors have been developed. This involves the application of static and Hopf bifurcation theory for PDE's and the very precise determination of steady state profiles. Practical computational methods for carrying out this analysis are discussed in some detail. For the special case of a first order, irreversible reaction in a tubular reactor with axial dispersion, the bifurcation behavior is classified and summarized in parameter space plots. In particular the influence of the Lewis and Peclet numbers is investigated. It is shown that oscillations due to interaction of dispersion and reaction effects should not exist in fixed bed reactors and moreover, should only occur in very short "empty" tubular reactors. The parameter study not only brings together previously published examples of multiple and periodic solutions but also reveals a hitherto undiscovered wealth of bifurcation structures. Sixteen of these structures, which come about by combinations of as many as four bifurcations to multiple steady states and four bifurcations to periodic solutions, are illustrated with numerical examples. Although the analysis is based on the pseudohomogeneous axial dispersion model, it can readily be applied to other reaction diffusion equations such as the general two phase models for fixed bed reactors.

AMS(MOS) Subject Classification: 35B32, 35K60,65N30, 65N35, 80A30

Key words: Bifurcation, partial differential equations, chemical reactors, computational methods

Work Unit No. 2 - Physical Mathematics

[†]Present address: Department of Chemical Engineering and Material Science, University of Minnesota, Minneapolis, MN 55455.

[*]Department of Chemical Engineering, University of Wisconsin, Madison, Wisconsin 53706.

Sponsored by the United States Army under Contract No. DAAG29-80-C-0041 and the National Science Foundation under Grant No. CPE79-21510.

SIGNIFICANCE AND EXPLANATION

Although the theory of static and Hopf bifurcation for nonlinear distributed parameter systems has been essentially developed, computational procedures easily used by applied mathematicians and engineers are required to bring these results into practice. The object of the present study is to show how the static and Hopf bifurcation behaviour for highly nonlinear processes may be determined as a function of process parameters. Special numerical methods are required to handle the very stiff steady state equations often encountered. Then special methods are demonstrated for mapping the parameter dependence of the bifurcation points. The direction and stability nature of the oscillatory solutions arising at Hopf bifurcation points is not determined here. However Poore and Heinemann [1980] describe an algorithm for this calculation.

The computational procedures are illustrated by application to an important problem found in chemical engineering: the dynamic behaviour of tubular reactors. Regions in parameter space are determined showing where static and Hopf bifurcations (both single and multiple) occur. The engineering significance of the results for this example problem is discussed.

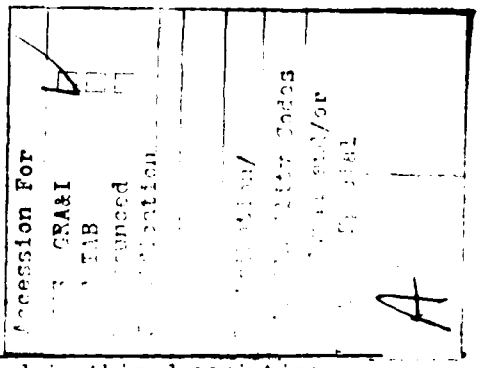

THE BIFURCATION BEHAVIOR OF TUBULAR REACTORS

Klavs F. Jensen[†] and W. Harmon Ray[*]

1. INTRODUCTION

In fixed bed reactors the reactants flow in gaseous or liquid form through a vessel (generally cylindrical in shape) packed with solid catalyst particles within which the reaction takes place. In the absence of catalyst packing, the vessel only serves to confine the reaction medium and it is then known as the "empty" tubular reactor. Naturally, the complex transport and reaction processes allow for different levels of sophistication in the mathematical modelling necessary to design and optimize fixed bed reactors [1-5]. Since these reactors moreover are used in a vast number of industrially important reactions [1, Table 1], they have received considerable attention during the last two decades. In particular, the occurrence of multiple steady states, travelling waves, and oscillatory states in these reactors has been a focal point in many theoretical and experimental investigations (cf. [5-12] for an overview). These phenomena were predicted by theoretical analyses before being consciously noted in experiments.

Table 1 gives a listing of experimental studies where multiple steady states (M), so-called wandering profiles (W), and oscillating behavior (O) were reported. Following Schmitz [9] we have omitted studies where the reactor was of the recirculating type which behaves more like a continuously stirred tank reactor (CSTR) than a fixed bed reactor. The publication dates of the entries in the table clearly demonstrate the recent growth in experimental evidence for bifurcation phenomena in fixed bed reactors.

[†]Present address: Department of Chemical Engineering and Material Science, University of Minnesota, Minneapolis, MN 55455.

[*]Department of Chemical Engineering, University of Wisconsin, Madison, Wisconsin 53706.

Sponsored by the United States Army under Contract No. DAAG29-80-C-0041 and the National Science Foundation under Grant No. CPE79-21510.

Table 1 Experimental studies of steady state multiplicity and instabilities in tubular reactors

Reference	Experimental System	Remarks
1. Volter, 1964 [13]	Polymerization of ethylene in a nonadiabatic tubular reactor	O
2. Padberg and Wicke, 1967, 1968 [14]	Oxidation of CO on Pt/Al_2O_3 in an adiabatic fixed bed reactor	M,W
3. Wicke et al., 1968 [15]	Oxidation of ethane on Pd/Al_2O_3 and oxidation of CO on Pt/Al_2O_3 in adiabatic fixed bed reactors	M,W
4. Root and Schmitz, 1969, 1970 [16]	Liquid phase reaction between $Na_2S_2O_3$ and H_2O_2 in a tubular reactor with recycle	M
5. Fieguth and Wicke, 1971 [17]	Oxidation of CO on Pt/Al_2O_3in a fixed bed reactor	M
6. Luss and Medellin, 1972 [18]	Liquid phase reaction between $Na_2S_2O_3$ and H_2O_2 in a tubular reactor with countercurrent flow of cooling in an annulus	M
7. Butakov and Maksimov, 1973 [19]	Liquid phase polymerization of styrene in a nonadiabatic tubular reactor	M
8. Hlaváček and Votruba, 1974 [20]	Oxidation of CO on Pd/Al_2O_3 and CuO/Al_2O_3 in an adiabatic fixed bed reactor	M
9. Renken et al., 1975 [21]	Hydrogenation of ethylene on Pt/Al_2O_3 in a fixed bed reactor	O,M
10. Stephens, 1975 [22]	Methanol synthesis in industrial autothermal fixed bed reactors	M
11. Hlaváček et al., 1976 [23]	Oxidation of CO on CuO/Al_2O_3, Pd/Al_2O_3 and Pt/Al_2O_3 in an adiabatic fixed bed reactor	M
12. Votruba et al., 1976 [24]	Oxidation of CO on Pt/Al_2O_3 and $CuO/Al_2/O_3$ in an adiabatic fixed bed reactor	M
13. Ampaya and Rinker, 1977 [25]	Water-gas shift reaction on Fe_3O_4/Cr_2O_3 in an autothermal fixed bed reactor	M

Table 1 (Cont.)

	Reference	Experimental System	Remarks
14.	Hegedus et al., 1977 [26]	Oxidation of CO on Pt/Al_2O_3 in an isothermal fixed bed reactor	M[1]
15.	Schleppy and Shah, 1977 [27]	NO reduction with CO over fiberglass supported Ru in a nonadiabatic fixed bed reactor	M
16.	Butakov and Shkadinskii, 1978 [28]	Liquid phase decomposition of dinitroxydiethylnitramine in acetic anhydride in a tubular reactor	O
17.	Hlaváček and Votruba, 1978 [12]	Oxidation of CO on CuO/Al_2O_3, Pd/Al_2O_3 and Pt/Al_2O_3 in an adiabatic reactor	M
18.	Oh et al., 1978 [29]	Oxidation of CO on Pt/Al_2O_3 in an isothermal fixed bed reactor	M[1]
19.	Aikus et al., 1979 [30]	Oxidation of CO on Pt/Al_2O_3 in an adiabatic fixed bed reactor	M
20.	Oh et al., 1979 [31]	Oxidation of CO on Pt/Al_2O_3 in an isothermal fixed bed reactor	M[1]
21.	Sharma and Hughes, 1979b [32]	Oxidation of CO on a CuO-catalyst in an adiabatic fixed bed reactor	M
22.	Hlaváček et al., 1980 [33]	Oxidation of CO on Pt/Al_2O_3 in a deactivated fixed bed reactor	M
23.	Kalthoff and Vortmeyer, 1980 [34]	Oxidation of ethane on Pd/Al_2O_3 in a nonadiabatic fixed bed reactor	M
24.	Paspek and Varma, 1980 [35]	Oxidation of ethylene on Pt/Al_2O_3 in a nonadiabatic fixed bed reactor	M
25.	Puszynski and Hlaváček, 1980 [36]	Oxidation of CO on Pt/Al_2O_3 in a nonadiabatic fixed bed reactor	M,W

M : multiple steady states
O : self-sustained oscillations
W : special investigation of "wandering"-profiles
1) short catalyst bed - approximately 8 catalyst layers

Because of the complex transport and reaction processes in fixed bed reactors, multiple steady states are generated by various kinetic and physicochemical mechanisms. The observed multiplicity behavior in the liquid phase reactions (entries 4 and 6) has been shown to follow the predictions of a plug flow reactor in a recycle loop. Naturally, the multiplicity of states in the autothermal reactors (entries 10 and 13) can be attributed to the feedback of heat through the preheating loop. In the studies by Hegedus, Oh and their coworkers (entries 14, 18, and 20) the multiple profiles stem from multiple steady states of the individual catalyst particles. Because the bed contains relatively few particles, the investigators are able to realize a number of stable profiles. Paspek and Varma (entry 24) also attribute the multiplicity behavior to the individual catalyst particles and explain the phenomenon in terms of interactions between the reaction and intraphase transport processes.

In the cases corresponding to the remaining entries in Table 1, dispersion effects seem to be part of the underlying mechanism. Hlaváček, Votruba and their respective coworkers (entries 8, 11, 12, 17, and 22) studied extensively the effects of reaction conditions on the multiplicity behavior in CO-oxidation and found that the phenomenon disappeared beyond a critical length (corresponding to $Pe_m \sim 180$) where the dispersion effects became insignificant. However, they also observed three stable profiles in their adiabatic reactor contrary to the theoretical prediction from the pseudo-homogeneous dispersion model of a maximum of two stable profiles. On the other hand, Sharma and Hughes (entry 21)

studying the same catalytic system could not realize more than the predicted two stable profiles. These authors found that a two phase axial dispersion model was required to accurately model their experimental data, whereas Schleppy and Shah (entry 15) showed for a different reaction system that the pseudohomogeneous axial dispersion model sufficed to fit the observed ignition and quench behavior. Kalthoff and Vortmeyer (entry 23) also used a pseudohomogeneous model but found it necessary to include the radial porosity and velocity distributions in order to quantitatively model the observed multiplicity behavior.

Wicke and his coworkers (entries 2 and 3) demonstrated the existence of travelling wave fronts, so-called wandering profiles, which moved slowly (linear velocity $\sim 10^{-3}$ cm/sec) and with small changes in shape through the reactor for changes in the gas velocity. For high gas velocities, the front was blown out, while for low velocities the front moved upstream to the reactor inlet. An intermediate velocity stabilized the front in the middle of the reactor. The travelling fronts are characterized by steep concentration and temperature gradients and most likely represent transitions between multiple steady state profiles. Transients reported by Sharma and Hughes (entry 21) as well as by Puszynski and Hlaváček (entry 25) nicely demonstrate the moving front structures which come about during the transition between states.

Oscillatory states in tubular reactors are reported in three experiments, entries 1, 9 and 16, but only in the last case are the oscillations linked to a mathematical model,

namely the axial dispersion model. The lack of experimental evidence of oscillatory profiles in fixed bed reactors may be explained by the fact that the characteristic time for thermal transport within the bed is so much larger than the one for material transport, i.e. the Lewis number is so large that oscillations are not expected even in shallow beds. This point will be treated in more detail below.

The question of uniqueness of the solution to the fixed bed reactor equations has been considered by numerous investigators, notably Amundson, Hlaváček and their respective coworkers. The axial dispersion model with a single first order reaction has been a favorite target for mathematical analyses and sufficient conditions for uniqueness have been developed by applying fixed point methods, comparison theorems, bifurcation theory, and Liapunov functionals. These contributions and others dealing with alternative models are reviewed by Jensen [37], Ray [7], Schmitz [9], and Varma and Aris [11]. The sufficient conditions for uniqueness, in the general case of a nonadiabatic reactor with unequal Peclet numbers for heat and mass dispersion, show (as intuitively expected) that the solution will be unique for sufficiently high values of the Peclet numbers, large heat transfer coefficients, or small values of the Damköhler number. Extensive calculations by Hlaváček and his coworkers [38-43] confirm this and show, in addition, that increasing the adiabatic temperature rise or the activation energy enlarges the region of multiplicity and shifts it towards lower Damköhler numbers, while an increase in the reaction order reduces the region of multiplicity. Multiplicity higher than three is possible only in the non-

adiabatic reactor, where five steady states have been calculated [40,44,45]. Recently, Kapila et al. [46] have shown by using activation energy asymptotics that as many as seven steady states may exist in the limit of large activation energy.

Also the travelling reaction fronts have generated much theoretical interest. Vortmeyer et al. [47-49] consider the reactor infinitely long which seems to be a reasonable assumption because the concentration and temperature changes in the front occur over very small distances compared to the reactor length. Gilles [50], in addition, approximated the reaction rate over the front zone by a Gaussian distribution. Rhee et al. [51,52] employed two-phase cell and continuum models and developed explicit formulae for the velocity similar to that for a shock layer in a nonreactive system. The above approaches all showed good agreement with experimental data.

The stability of the steady state has been studied numerically by linearization where the dominant eigenvalues were determined from either a collocation or Galerkin approximation to the linearized equations [44,45,53,54]. Alternatively sufficient conditions for stability have been derived through the use of comparison theorems and Liapunov functionals [55-63].

As expected from the physical situation and formally shown by singular perturbation theory [64,65], the pseudohomogeneous axial dispersion model reduces to the CSTR model as the Peclet number becomes very small. Therefore, based on the dynamic behavior of the CSTR [cf. 66,67] one expects oscillations to exist in short reactors. The existence of such oscillations in the "empty" tubular reactor has been determined computationally

by Hlaváček and Hofmann [39] and Varma and Amundson [45b]. However, examples have not been calculated for fixed bed reactors. A detailed parametric study has not yet been performed for either type of reactor; thus, in this paper we shall show how such a study can be made by using bifurcation theory. We shall be especially concerned with the effect of the Lewis number, i.e. the ratio of physical transport thermal time constant to physical transport material time constant. This parameter, which is unity for the empty tubular reactor and much greater than unity for fixed bed reactors, has been shown to have a striking influence on the dynamics of chemically reacting systems (cf. [67] and references within). Therefore, the analysis will have practical interest in revealing if limit cycles are at all possible even in short fixed bed reactors. Although the bifurcation analysis, i.e. the study of multiple steady states and oscillatory behavior, will be based on the pseudohomogeneous axial dispersion model with first order Arrhenius kinetics, the general approach readily applies to other reaction-diffusion equations with complex rate expressions. The dispersion model is a particularly good example for illustrating the techniques since the modelling equations form a relatively simple set of nonlinear parabolic differential equations which are capable of predicting multiple steady states and limit cycles. Moreover, stiffness problems are often encountered in the numerical solution to the steady state equations which means that one has to devise versatile and efficient algorithms. Finally, the previously published examples of multiple steady states [e.g. 38-41,45] make it possible to check the algorithms.

2. MODELLING EQUATIONS

In the case of an irreversible first order reaction, the equations of the pseudohomogeneous axial dispersion model are two coupled nonlinear parabolic partial differential equations for the reactant concentration and the temperature [2,11]. The equations are:

$$\varepsilon_p \frac{\partial c(z',t')}{\partial t'} = D_L \frac{\partial^2 c(z',t')}{\partial z'^2} - v_z \frac{\partial c(z',t')}{\partial z'} - k_0(1-\varepsilon_p)c(z',t')\exp[-E_A/RT(z',t')] \qquad (1)$$

$$[\varepsilon_p \rho_f C_{pf} + (1-\varepsilon_p)\rho_s C_{ps}]\frac{\partial T(z',t')}{\partial t'} = k_L \frac{\partial T^2(z',t')}{\partial z'^2} - \rho_f C_{pf} v_z \frac{\partial T(z',t')}{\partial z'} + (1-\varepsilon_p)(-\Delta H_r)k_0 c(z',t')\exp[-E_A/RT(z',t')] - \frac{4}{d_r}U_w[T(z',t')-T_w(z',t')] \qquad (2)$$

with initial conditions

$$c(z',0) = c_{in}(z') , \quad T(z',0) = T_{in}(z') \qquad (3)$$

Here we use Danckwerts' boundary conditions, even in the analysis of the transients.

$$-D_L \left.\frac{\partial c(z',t')}{\partial z'}\right|_0 = v_z[c_0(t') - c(0,t')] \qquad (4a)$$

$$\left.\frac{\partial c(z',t')}{\partial z'}\right|_\ell = 0 \qquad (4b)$$

$$-k_L \left.\frac{\partial T(z',t')}{\partial z'}\right|_0 = v_z \rho_f C_{pf}[T_0(t') - T(0,t')] \qquad (5a)$$

$$\left.\frac{\partial T(z',t')}{\partial z'}\right|_\ell = 0 \qquad (5b)$$

In the above equations c and T represent the concentration and temperature. D_L and k_L are the longitudinal dispersion coefficients, while v_z is the gas velocity. Subscripts f, s, and w denote the fluid phase, solid phase, and reactor wall respectively. ε_p and d_r are the bed porosity and diameter. k_0 and E_A represent the usual Arrhenius parameters. U_w is the overall heat transfer coefficient between the reactor and cooling medium. The effect of radial heat dispersion may be included in U_w by making a one-point collocation approximation to the radial temperature profile [80].

The equations are made dimensionless by defining:

$$x_1 = \frac{c-c_0}{c_0} \quad , \quad x_2 = \left(\frac{T-T_0}{T_0}\right)\frac{E_A}{RT_0} \quad , \quad x_{2w} = \left(\frac{T_w-T_0}{T_0}\right)\frac{E_A}{RT_0} \quad , \quad \gamma = \frac{E_A}{RT_0} \quad ,$$

$$t = \frac{t' v_z}{\varepsilon_p \ell} \quad , \quad z = \frac{z'}{\ell} \quad , \quad Pe_1 = \frac{v_z \ell}{D_L} \quad , \tag{6}$$

$$Pe_2 = \frac{v_z \ell \rho_f C_{pf}}{k_L} \quad , \quad Da = \frac{\ell(1-\varepsilon_p)k_0 e^{-\gamma}}{v_z} \quad , \quad B = \frac{(-\Delta H)c_0\gamma}{\rho_f C_{pf} T_0} \quad ,$$

$$\beta = \frac{4\ell U_w}{v_z d_r \rho_f C_{pf}} \quad , \quad Le = \frac{\varepsilon_p \rho_f C_{pf} + (1-\varepsilon_p)\rho_s C_{ps}}{\rho_f C_{pf} \varepsilon_p}$$

We then obtain the following set of equations:

$$\underline{\underline{C}} \frac{\partial \underline{x}}{\partial t} = \underline{\underline{L}}\underline{x} + \underline{f}(\underline{x}) \tag{7}$$

where $\underline{\underline{C}}$ denotes the capacity matrix

$$\underline{\underline{C}} = \begin{bmatrix} 1 & 0 \\ 0 & Le \end{bmatrix} \tag{8}$$

and $\underset{\sim}{L}$ denotes the linear differential operator:

$$\underset{\sim}{L} = \begin{bmatrix} Pe_1^{-1} & 0 \\ 0 & Pe_2^{-1} \end{bmatrix} \frac{\partial^2}{\partial z^2} - \begin{bmatrix} 1 & 0 \\ 0 & 1 \end{bmatrix} \frac{\partial}{\partial z} - \begin{bmatrix} 0 & 0 \\ 0 & \beta \end{bmatrix} \tag{9}$$

The nonlinearity $\underset{\sim}{f}(\underset{\sim}{x})$ is:

$$\underset{\sim}{f}(\underset{\sim}{x}) = \begin{bmatrix} Da(1-x_1)\exp\left[\dfrac{x_2}{1+x_2/\gamma}\right] \\ B\ Da(1-x_1)\exp\left[\dfrac{x_2}{1+x_2/\gamma}\right] + \beta x_{2w} \end{bmatrix} \tag{10}$$

In this formulation the boundary conditions take the form:

$$\underset{\sim}{B}_1\underset{\sim}{x}(0,t) = \begin{bmatrix} \dfrac{\partial}{\partial z} - Pe_1 & 0 \\ 0 & \dfrac{\partial}{\partial z} - Pe_2 \end{bmatrix} \underset{\sim}{x}(\ ,t) = \underset{\sim}{0} \tag{11a}$$

$$\underset{\sim}{B}_2\underset{\sim}{x}(1,t) = \begin{bmatrix} \dfrac{\partial}{\partial z} & 0 \\ 0 & \dfrac{\partial}{\partial z} \end{bmatrix} \underset{\sim}{x}(1,t) = \underset{\sim}{0} \tag{11b}$$

In the special adiabatic case with Le = 1, the modelling equations may be reduced to one equation. This is done by multiplying the mass balance by B and subtracting it from

the energy balance to give an equation whose only solution is

$$x_2 = Bx_1 \tag{12}$$

This relationship makes the reaction rate a function of only one variable.

The parameters each have specific physical meaning. The quantity B is a dimensionless adiabatic temperature rise and Da represents the ratio of reactor space time to the characteristic reaction time. Pe_1 and Pe_2 are the Peclet numbers for mass and heat transport and β is a dimensionless heat transfer coefficient. As mentioned, Le is the ratio of the physical transport thermal time constant to the physical transport material time constant [67].

Based on common exothermic reactions, Hlaváček and Votruba [5, Table 6.6] list values of B and γ in the range 5-30 where the high values of B usually correspond to oxidation reactions. For the "empty" tubular reactor $Le = 1$, while for a typical fixed bed reactor $Le \sim 500$. When the reactor is empty, $Pe_1 \tilde{=} Pe_2$, while for the packed reactor, $Pe_1 \sim$ 2-3 times Pe_2 since the value of Pe_2 derives from the width of the reaction zone as well as the length of the reactor. This implies that multiplicity is possible even in long reactors (cf. [41]). The Damköhler number, Da, and the dimensionless heat transfer coefficient, β, vary with the reactor space time but are usually less than 0.5 and 5 respectively.

3. BIFURCATION ANALYSIS

Bifurcation, or branching of solutions, is closely related to the stability and thus to the eigenvalues of linearized system

equations. As an example, consider the system of nonlinear coupled ODEs

$$\frac{d\underset{\sim}{x}}{dt} = \underset{\sim}{F}(\underset{\sim}{x},\underset{\sim}{p})$$

where $\underset{\sim}{x}$ is a state vector and $\underset{\sim}{p}$ represents a vector of parameters. The system is locally stable if all eigenvalues of the Jacobian have negative real parts. The eigenvalues are functions of the system parameters and these may change such that the system loses its stability. The exchange of stability occurs as some eigenvalues cross the imaginary axis, and it is at this point that the bifurcation can take place. Therefore, bifurcation is often referred to as "the principle of exchange of (linearized) stability" (cf. [68] for a detailed discussion of this). There are two ways in which the eigenvalues can cross the imaginary axis, namely:

(i) A simple eigenvalue passes through the origin. This leads to bifurcation of stationary solutions and is known as "static bifurcation" [69].

(ii) A pair of simple complex conjugate eigenvalues cross the imaginary axis. This leads to bifurcation of periodic solutions and is known as "Hopf-bifurcation" (cf. [70] for more details).

Occasionally multiple eigenvalues cross the imaginary axis together and this may produce complex interactions between the two basic bifurcation phenomena (cf. [70,71] for examples).

Because partial differential equations (PDEs) can be regarded in some aspects as an infinite set of ODEs, one intuitively expects, and can in fact show, under certain

limited conditions [71-75 and references within], that the bifurcation theorems for ODEs can be extended to the "infinite dimensional case". The review paper by Crandall [75] gives a particularly readable account of the necessary concepts and proofs. The conditions are all satisfied for the parabolic or elliptic partial differential equations which arise in reaction-diffusion problems.

We now linearize the equations around a spatially varying steady state profile rather than a point as in the ODE case. The linearized equations take the form:

$$\underset{\sim}{C}\frac{\partial \bar{\underset{\sim}{x}}}{\partial t} = \underset{\sim}{L}\bar{\underset{\sim}{x}} + \left.\frac{\partial \underset{\sim}{f}(\underset{\sim}{x})}{\partial \underset{\sim}{x}}\right|_{\substack{\bar{\underset{\sim}{x}}(z) \\ \underset{\sim}{x}(z)=\underset{\sim}{x}_s(z)}} \tag{13}$$

$$\underset{\sim}{B}_0\bar{\underset{\sim}{x}}(0) = \underset{\sim}{o} \tag{14}$$

$$\underset{\sim}{B}_1\bar{\underset{\sim}{x}}(1) = \underset{\sim}{o} \tag{15}$$

where $\bar{\underset{\sim}{x}} = \underset{\sim}{x}-\underset{\sim}{x}_s$ and $\underset{\sim}{C}$, $\underset{\sim}{L}$, $\underset{\sim}{f}$, $\underset{\sim}{B}_0$, and $\underset{\sim}{B}_1$ are defined by equations (8), (9), (10), and (11) respectively. The branching to nontrivial solutions or periodic solutions is then governed by the discrete spectrum, i.e. the eigenvalues, of the linear operator:

$$\underset{\sim}{F}_x = \underset{\sim}{C}^{-1}\left[\underset{\sim}{L} + \left.\frac{\partial \underset{\sim}{f}(\underset{\sim}{x})}{\partial \underset{\sim}{x}}\right|_{\underset{\sim}{x}=\underset{\sim}{x}_s}\right] \tag{16}$$

Analogously to the ODE case, one sees:

(i) Static bifurcation, when a simple eigenvalue in the spectrum passes through the origin.

(ii) Hopf-bifurcation, when a simple pair of complex eigenvalues in the spectrum passes the imaginary axis.

In addition, there must be an exchange of stability at the bifurcation point; e.g., in order to have Hopf-bifurcation, the remaining eigenvalues must have negative real parts. The first N eigenvalues of $\underset{\sim}{F}_{\hat{x}}$ may be determined by using projection techniques such as Galerkin's method orthogonal collocation. In the limit of infinite terms, both methods will represent $\underset{\sim}{F}_x$ exactly [76,77]. Thus, this "late lumping" procedure retains all the information in the original partial differential equations, contrary to the behavior of the "early lumping" procedures such as Hlaváček's "linearization" [38] which, for example, cannot predict the existence of more than three steady states. For both the collocation and the Galerkin method the finite dimensional Jacobian takes the form:

$$\underset{\sim}{J} = \begin{bmatrix} \underset{\sim}{M}_1+\underset{\sim}{K}_{11} & \underset{\sim}{K}_{12} & & & \\ \underset{\sim}{K}_{21} & \underset{\sim}{M}_2+\underset{\sim}{K}_{22} & & & \\ & & \ddots & & \\ & & & \underset{\sim}{M}_{N-1}+\underset{\sim}{K}_{N-1\,N-1} & \underset{\sim}{K}_{N+N} \\ & & & \underset{\sim}{K}_{NN-1} & \underset{\sim}{M}_N+\underset{\sim}{K}_{NN} \end{bmatrix} \tag{17}$$

where N is the number of eigenfunctions in the Galerkin method or the number of interior collocation points in the collocation method.

The quantities $\underset{\sim}{M}_i$ and $\underset{\sim}{K}_{ij}$ are 2 x 2 matrices defined below (except in the special adiabatic case with $Le = 1$, where they are scalars). In the following we shall describe our approach to this analysis using weighted residual methods [77].

(i) Galerkin's method

We make the usual transformation which causes the problem to become self adjoint [62]:

$$\bar{x}_k^* = \bar{x}_k \exp\left\{-\frac{Pe_k}{2} z\right\}, \quad k = 1,2 \tag{18}$$

and choose the trial function expansion:

$$\bar{x}_k^* = \sum_{i=1}^{N} a_{ki}(t)\, \phi_{ki}(z), \quad k = 1,2 \tag{19}$$

where the $\phi_{ki}(z)$ are the orthonormal eigenfunctions corresponding to the self adjoint eigenvalue problem:

$$\frac{d^2\phi_{kn}}{dz^2} = -\lambda_{kn}\phi_{kn} \tag{20}$$

$$\left.\frac{d\phi_{kn}}{dz}\right|_{z=0} = \frac{Pe_k}{2}\,\phi_{kn}(z=0) \tag{21a}$$

$$\left.\frac{d\phi_{kn}}{dz}\right|_{z=1} = -\frac{Pe}{2}\,\phi_{kn}(z=1) \tag{21b}$$

hence

$$\phi_{kn}(z) = \{2/[\lambda_{kn} + Pe_k + (Pe_k^2/4)]\}^{1/2}\{\sqrt{\lambda_{kn}}\cos(\sqrt{\lambda_{kn}}z) + (Pe_k/2)\sin(\sqrt{\lambda_{kn}}z)\} \tag{22}$$

where the eigenvalues, λ_{kn}, are the zeros of the transcendental equation:

$$\tan\sqrt{\lambda_{kn}} = \frac{Pe_k\sqrt{\lambda_{kn}}}{\lambda_{kn} - (Pe_k/2)^2} \tag{23}$$

By inserting the trial functions into the linearized equations and making the resulting residuals orthogonal to the first N eigenvalues, one obtains the following system of ODEs:

$$\frac{d\underset{\sim}{a}(t)}{dt} = \underset{\sim}{J}\underset{\sim}{a}(t) \tag{24}$$

where $a = (a_{11}, a_{21}, a_{12}, a_{22}, \cdots a_{1N}, a_{2N})^T$ and $\underset{\sim}{J}$ is defined by (17) with

$$\underset{\sim}{M}_i = \begin{bmatrix} \left[\frac{\lambda_{1i}}{Pe_1} + \frac{Pe_1}{4}\right] & 0 \\ 0 & -\frac{1}{Le}\left[\frac{\lambda_{2i}}{Pe_2} + \frac{Pe_2}{4} + \beta\right] \end{bmatrix} \tag{25}$$

and

$$\underset{\sim}{K}_{ij} = \begin{bmatrix} \int_0^1 \left.\frac{\partial f_1}{\partial x_1}\right|_{\underset{\sim}{x}=\underset{\sim}{x}_s} \phi_{1i}\phi_{1j}dz & \int_0^1 \left.\frac{\partial f_1}{\partial x_2}\right|_{\underset{\sim}{x}=\underset{\sim}{x}_s} \exp[\tfrac{z}{2}(Pe_2-Pe_1)]\phi_{2i}\phi_{1j}dx \\ \frac{1}{Le}\int_0^1 \left.\frac{\partial f_2}{\partial x_1}\right|_{\underset{\sim}{x}=\underset{\sim}{x}_s} \exp[\tfrac{z}{2}(Pe_1-Pe_2)]\phi_{1i}\phi_{2j}dz & \frac{1}{Le}\int_0^1 \left.\frac{\partial f_2}{\partial x_2}\right|_{\underset{\sim}{x}=\underset{\sim}{x}_s} \phi_{2i}\phi_{2j}dz \end{bmatrix} \tag{26}$$

Note that $\underset{\sim}{K}_{ij} = \underset{\sim}{K}_{ji}$.

(ii) The Orthogonal Collocation Method

This method has been successfully applied to many chemical reaction engineering problems similar to the present eigenvalue problem [53,54,78-81]. In this method the first and second spatial derivatives are approximated by a weighted sum of the values of the dependent variable at the collocation points:

$$\left.\frac{\partial x_k}{\partial z}\right|_{z_i} = \sum_{j=0}^{N+1} A_{ij} x_{kj} \quad ; \quad i = 0,1,\ldots,N, N+1 \; ; \quad k = 1,2 \qquad (27)$$

and

$$\left.\frac{\partial^2 x_k}{\partial z^2}\right|_{z_i} = \sum_{j=0}^{N+1} B_{ij} x_{kj} \quad ; \quad i = 0,1,\ldots,N, N+1 \; ; \quad k = 1,2 \qquad (28)$$

The weight matrices depend on the trial functions which in our case are the first N Jacobi polynomials $P_i^{(\alpha,\beta)}(z)$ with weight function $z^{\alpha}(1-z)^{\beta}$ [81, ct. 3]. Since there is no special symmetry in the tubular reactor problem, we use $(\alpha,\beta) = (0,0)$ in which case the polynomials are Legendre polynomials. In fact, Georgakis et al. [54] compared the convergence rate of the eigenvalue calculations for various choices of α and β and found that the fewest number of collocation points were required for $\alpha = \beta = 0$. The collocation points are then the zeros of $P_N^{(0,0)}(z)$. By discretizing the equations and eliminating the boundary conditions (as detailed in [54 ,81 ct. 4]), we obtain the following set of ordinary differential equations:

$$\frac{d\underset{\sim}{y}}{dt} = \underset{\sim}{J}\underset{\sim}{y} \qquad (29)$$

where the eigenvalues, λ_{kn}, are the zeros of the transcendental equation:

$$\tan\sqrt{\lambda_{kn}} = \frac{Pe_k\sqrt{\lambda_{kn}}}{\lambda_{kn} - (Pe_k/2)^2} \tag{23}$$

By inserting the trial functions into the linearized equations and making the resulting residuals orthogonal to the first N eigenvalues, one obtains the following system of ODEs:

$$\frac{d\underset{\sim}{a}(t)}{dt} = \underset{\sim\sim}{J}\underset{\sim}{a}(t) \tag{24}$$

where $a = (a_{11}, a_{21}, a_{12}, a_{22}, \ldots a_{1N}, a_{2N})^T$ and $\underset{\sim}{J}$ is defined by (17) with

$$\underset{\sim}{M}_i = \begin{bmatrix} \left[\frac{\lambda_{1i}}{Pe_1} + \frac{Pe_1}{4}\right] & 0 \\ 0 & -\frac{1}{Le}\left[\frac{\lambda_{2i}}{Pe_2} + \frac{Pe_2}{4} + \beta\right] \end{bmatrix} \tag{25}$$

and

$$\underset{\sim}{K}_{ij} = \begin{bmatrix} \int_0^1 \left.\frac{\partial f_1}{\partial x_1}\right|_{\underset{\sim}{x}=\underset{\sim}{x}_s} \phi_{1i}\phi_{1j}dz & \int_0^1 \left.\frac{\partial f_1}{\partial x_2}\right|_{\underset{\sim}{x}=\underset{\sim}{x}_s} \exp[\tfrac{z}{2}(Pe_2-Pe_1)]\phi_{2i}\phi_{1j}dx \\ \frac{1}{Le}\int_0^1 \left.\frac{\partial f_2}{\partial x_1}\right|_{\underset{\sim}{x}=\underset{\sim}{x}_s} \exp[\tfrac{z}{2}(Pe_1-Pe_2)]\phi_{1i}\phi_{2j}dz & \frac{1}{Le}\int_0^1 \left.\frac{\partial f_2}{\partial x_2}\right|_{\underset{\sim}{x}=\underset{\sim}{x}_s} \phi_{2i}\phi_{2j}dz \end{bmatrix} \tag{26}$$

Note that $\underset{\sim}{K}_{ij} = \underset{\sim}{K}_{ji}$.

(ii) The Orthogonal Collocation Method

This method has been successfully applied to many chemical reaction engineering problems similar to the present eigenvalue problem [53,54,78-81]. In this method the first and second spatial derivatives are approximated by a weighted sum of the values of the dependent variable at the collocation points:

$$\left.\frac{\partial x_k}{\partial z}\right|_{z_i} = \sum_{j=0}^{N+1} A_{ij} x_{kj} \quad ; \quad i = 0,1,\ldots,N, N+1 \; ; \quad k = 1,2 \tag{27}$$

and

$$\left.\frac{\partial^2 x_k}{\partial z^2}\right|_{z_i} = \sum_{j=0}^{N+1} B_{ij} x_{kj} \quad ; \quad i = 0,1,\ldots,N, N+1 \; ; \quad k = 1,2 \tag{28}$$

The weight matrices depend on the trial functions which in our case are the first N Jacobi polynomials $P_i^{(\alpha,\beta)}(z)$ with weight function $z^{\alpha}(1-z)^{\beta}$ [81, ct. 3]. Since there is no special symmetry in the tubular reactor problem, we use $(\alpha,\beta) = (0,0)$ in which case the polynomials are Legendre polynomials. In fact, Georgakis et al. [54] compared the convergence rate of the eigenvalue calculations for various choices of α and β and found that the fewest number of collocation points were required for $\alpha = \beta = 0$. The collocation points are then the zeros of $P_N^{(0,0)}(z)$. By discretizing the equations and eliminating the boundary conditions (as detailed in [54 ,81 ct. 4]), we obtain the following set of ordinary differential equations:

$$\frac{d\underline{y}}{dt} = \underline{\underline{J}}\,\underline{y} \tag{29}$$

where $\underset{\sim}{y} = (x_{11}, x_{21}, x_{12}, x_{22}, \ldots, x_{1N}, x_{2N})^T$ is the conversion and dimensionless temperature at N interior collocation points. $\underset{\sim}{J}$ is defined by (17) with:

$$\underset{\sim}{M}_i = \begin{bmatrix} \left.\frac{\partial f_1}{\partial x_1}\right|_{\underset{\sim}{x}=\underset{\sim}{x}_s(z_i)} & \left.\frac{\partial f_1}{\partial x_2}\right|_{\underset{\sim}{x}=\underset{\sim}{x}_s(z_i)} \\ \frac{1}{Le}\left.\frac{\partial f_2}{\partial x_1}\right|_{\underset{\sim}{x}=\underset{\sim}{x}_s(z_i)} & \frac{1}{Le}\left.\frac{\partial f_2}{\partial x_2}\right|_{\underset{\sim}{x}=\underset{\sim}{x}_s(z_i)} \end{bmatrix} \tag{30}$$

and

$$\underset{\sim}{K}_{ij} = \begin{bmatrix} \frac{B^*_{1ij}}{Pe_1} - A^*_{1ij} & 0 \\ 0 & \frac{1}{Le}\left[\frac{B^*_{2ij}}{Pe_j} - A^*_{2ij} - \delta_{ij}\,\beta\right] \end{bmatrix} \tag{31}$$

δ_{ij} is Kronecker's delta and $\underset{\sim}{A}^*$ and $\underset{\sim}{B}^*$ are the differentiation weight matrices corrected for the boundary conditions, (14) and (15), i.e.,

$$\begin{aligned} X^*_{kij} = {} & X_{ij} \\ & -[(A_{00}-Pe_k)A_{N+1,N+1}-A_{0,N+1}A_{N+1,0}]^{-1}[(A_{N+1,N+1}A_{0j}-A_{0,N+1}A_{N+1,j})X_{i0} \\ & + ((A_{00}-Pe_k)A_{N+1,j}-A_{N+1,0}A_{0j})X_{i,N+1}] \end{aligned} \tag{32}$$

$$X = A,B \qquad k = 1,2$$

The evaluation of the derivatives, $\left.\frac{\partial f_j}{\partial x_k}\right|_{z_i}$, usually requires interpolation among the discrete points of the steady state solution. The computational effort involved in the two procedures, (i) and (ii), are then nearly equivalent in spite of the integrals in (26) because the integrals can readily be evaluated by quadrature. The choice of method therefore strictly depends on their convergence properties. McGowin and Perlmutter [53] showed in numerical examples that Galerkin's method converged monotonically while the collocation procedure converged in a dampened oscillatory manner, but they did not compare the overall rate of convergence. Because of the similarity between the eigenfunction expansion and the perturbation solution to the special adiabatic case with Le = 1 [64,65], one expects that the necessary number of terms, N, will increase with the value of the Peclet number starting from N = 1 at small Peclet numbers. This is further discussed below.

4. CALCULATION OF THE STEADY STATE

The steady state equations for the reactor (cf. Equation (7)) form a nonlinear two point boundary value problem which is quite stiff even for moderate values of Peclet numbers (Pe ~ 10). This boundary value problem must be solved quickly and accurately if one wishes to obtain the bifurcation curves with judicious use of computing time. Therefore, we have given special consideration to the calculation of the steady state profiles.

Because of the stiffness, finite differences would require far too many mesh points and can thus be ruled out. Although efficient routines exist for solving stiff initial value

problems (e.g. [82,83]), the shooting methods of McGinnis [84] and Kubíček and Hlaváček [95] are cumbersome since they respectively require the integration of 12 and 24 first order equations. In addition, because of the marching nature of the technique, the solution must be stored in arrays in order to be used in the bifurcation analysis. On the other hand, in the method of weighted residuals the solution is characterized by a few trial functions. Moreover, as mentioned, the collocation approach has been proven to be very efficient in solving this type of boundary value problem. There are several ways this method may be applied and in the following paragraphs we review the advantages and disadvantages of these. More details on the computational procedures may be found elsewhere [37].

(i) Collocation over the whole domain, $0 \leq z \leq 1$, with orthogonal polynomials. This method is simple and has the advantage that the collocation points and weights need only be calculated once. It has been used successfully in cases of moderate values of the Peclet numbers ($Pe < 10$) [e.g. 54,79,80], but the procedure is inadequate at high values of Damköhler and Peclet numbers where the reaction is complete within a narrow zone close to the reactor inlet as illustrated in Figure 1. In order to obtain a good representation of the narrow reaction zone, a large number of collocation points are needed, most of which are wasted downstream from the reaction zone. Moreover, the large number of points cause the interpolating polynomial to wiggle as shown in Figure 1. Although the wiggles are slight, they significantly alter the bifurcation behavior. This is illustrated in Figure 2a, which shows the calculated regions of multiplicity. Note that the collocation technique with $N \geq 8$ can accurately represent

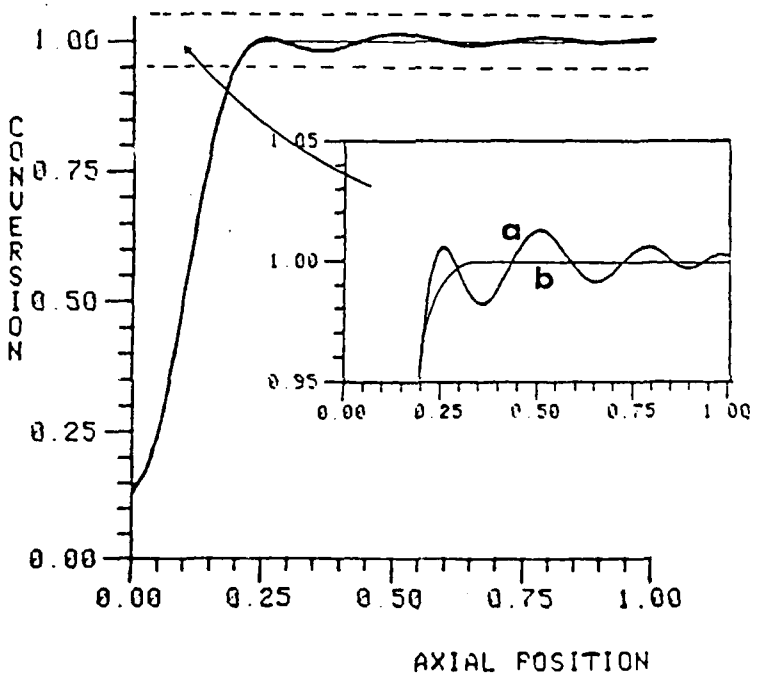

Figure 1 Behavior of the interpolating polynomial (a) compared to the exact solution (b). Approximate solution based on orthogonal collocation, M = 10. Reactor parameters: B = 10.0, Da = 0.13, $Pe_1 = Pe_2 = 15.0$, $\beta = 0.0$, $\gamma = 20.0$.

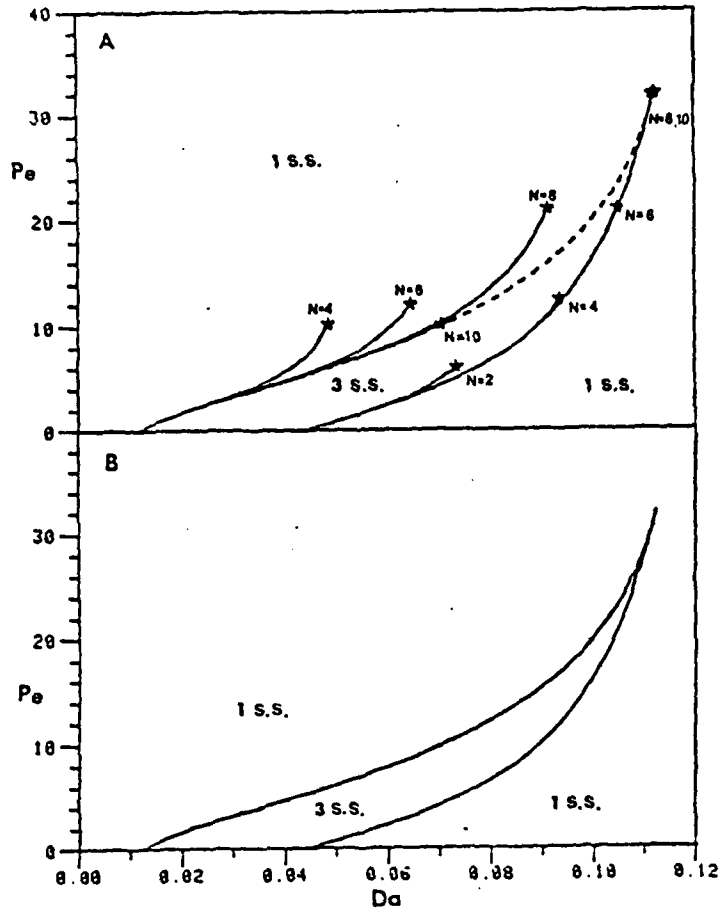

Figure 2 Static bifurcation curves based on steady state solutions with orthogonal collocation (A) and spline collocation (M = 10) (B); B = 10.0, β = 0.0, γ = 20.0.

the branch corresponding to the lower steady state, but even for $N = 10$, it cannot predict the steep upper steady state profiles when $Pe > 10$.

(ii) Transformation of the independent variable followed by collocation over the whole domain. In order to avoid using a large number of collocation points when the profiles are steep, a suitable transformation of the independent variable can be made such that the reaction zone is stretched and the "dead-zone" is compressed. This implies that the majority of the collocation points will be located in the region of rapid changes. However, no general transformation will fit the entire region transversed by the reaction front for changes in the bifurcation parameters, e.g. Da. The transformation must contain at least one adjustable parameter which has to be fitted to an approximate profile by nonlinear least squares. Our experience with this method indicates that the computations become too lengthy to act as a basis for the bifurcation analysis.

(iii) Orthogonal collocation with exponentials. Orthogonal collocation with trial functions of the form: $f_i(z) = z^{\alpha_i} e^{\beta_i z}$ have been shown to give excellent results in plug flow reactor problems since the trial functions are solutions to the corresponding linear problem [86]. Because the axial dispersion model in the limit of large Peclet numbers approaches the plug flow model, this approach should also be able to solve the stiff cases. However, we did not find any significant improvement over the standard procedure (i), presumably because of difficulties in determining an optimal choice for the coefficients, α_i and β_i. The optimal selection of these

coefficients remains an open problem [86]. The method has the further disadvantage that re-evaluation of the collocation points and the weight matrices is necessary after each change in the bifurcation parameter, which greatly increases computation time.

(iv) Orthogonal Spline Collocation (also referred to as orthogonal collocation of finite elements). This method has been successfully applied in other problems with steep gradients, notably the catalyst particle problem for large values of the Thiele modulus [81, cf. 7, 87,88]. The increased accuracy of this approach over the global approach (i) derives from the concentration of the collocation points in the regions where the gradients are steep. Since the number of points are reduced in the remaining regions where the solutions only change slightly, the total number of collocation points may be less than required in the standard case (i). In addition, by balancing the number of collocation points and spline intervals, one can obtain a patched interpolating polynomial of sufficiently low order that wiggles are avoided. The location of the spline points is clearly critical to the accuracy of the approach. Carey and Finlayson [87] suggested placing the elements such that the mean squared residual was minimized. After a given calculation the residuals were examined and new elements inserted where the residual had been largest. Then the procedure was repeated until the desired accuracy was reached. This approach is general but may give large array sizes. Instead, one may fix the number of spline points and let their location move with the reaction front as the bifurcation parameter changes. A simple way to accomplish

this is to monitor the gradients of the solution and place the spline points accordingly. However, this approach requires a priori knowledge of the shape of the profiles. A far more general approach is to rearrange the spline points such that the mean squared residual is minimized. This can be done by determining the sensitivity of the solution to the location of the spline point [37]. Because of the extra computations in the optimization of the spline point, the choice between this method and the one proposed by Carey and Finlayson depends on the relative importance of computer time and space requirements. However, for cases where the rate expression can be expressed as a function of a single reactant, the following simple procedure is attractive.

(v) A Simple Orthogonal Spline Collocation Method. This method only applies to problems where the reaction rate can be expressed in terms of one reactant, but because of its ability to give fast and accurate solutions, it is worthwhile considering. Moreover, many reactor studies involve such kinetics. The numerical difficulties are circumvented here by obtaining a collocation solution for the reaction zone and patching this together with an analytical solution for the remaining part of the reactor, the "dead-zone". Thus this procedure retains the advantages of the simple collocation procedures described in (i) above and in addition provides for concentrating the collocation points in the reaction zone.

If one assumes that the reaction is essentially complete beyond the spline point z_s, one may neglect the reaction rate term so that the steady state equations on the interval $z_s \leq z \leq 1$ become:

$$x_1 = 1 \tag{33}$$

and

$$x_2 = \beta \quad \text{if} \quad \beta = 0 \tag{34a}$$

$$\frac{1}{Pe_2}\frac{dx_2^2}{dz^2} - \frac{dx_2}{dz} - \beta(x_2 - x_{2w}) = 0 \quad \text{if} \quad \beta > 0 \tag{34b}$$

with the boundary condition

$$\left.\frac{dx_2}{dz}\right|_{z=1} = 0 \tag{35}$$

and the continuity condition

$$x_2\Big|_{z_s^-} = x_2\Big|_{z_s^+} = x_{2s} \tag{36}$$

where x_{2s} is specified once the solutions over the two zones are patched together. For constant x_{2w}, equation (34b) may be solved analytically:

$$\frac{x_2 - x_{2w}}{x_{2s} - x_{2w}} = \frac{\alpha_1 e^{-\alpha_2(1-z)} - \alpha_2 e^{-\alpha_1(1-z)}}{\alpha_1 e^{-\alpha_2(1-z_s)} - \alpha_2 e^{-\alpha_1(1-z_s)}} \tag{37}$$

where

$$\alpha_1, \alpha_2 = \frac{Pe_2}{2}\left[1 \pm \sqrt{1 + \frac{4\beta}{Pe_2}}\right] \tag{38}$$

With the variable change $\zeta = z/z_s$, the steady state equations governing the reaction zone take the form:

$$\frac{1}{Pe_k}\frac{d^2x_k}{d\zeta^2} - z_s\frac{dx_k}{d\zeta} + z_s^2[f_k(x_1, x_2) - \delta_{2k}\beta x_2] = 0 \; ; \quad k=1,2 \tag{39}$$

with boundary conditions:

$$\left.\frac{dx_k}{d\zeta}\right|_{\zeta=0} = z_s Pe_k x_k , \quad k=1,2 \tag{40}$$

and the continuity restrictions:

$$x_k\Big|_{\zeta=1^-} = x_k\Big|_{\zeta=1^+} \tag{41a}$$

$$\left.\frac{dx_1}{d\zeta}\right|_{\zeta=1} = 0 \tag{41b}$$

$$\left.\frac{dx_2}{d\zeta}\right|_{\zeta=1} = \begin{cases} 0 \quad \text{for} \quad \beta=0 \\ z_s(x_2\Big|_{\zeta=1} - x_{2w}) \dfrac{\alpha_1\alpha_2[e^{-\alpha_2(1-z_s)} - e^{-\alpha_1(1-z_s)}]}{\alpha_1 e^{-\alpha_2(1-z_s)} - \alpha_2 e^{-\alpha_1(1-z_s)}} & \text{for } \beta\neq 0 \end{cases} \tag{41c}$$

Following the standard collocation technique and eliminating the continuity and boundary conditions, one obtains the collocation equations:

$$\sum_{j=1}^{M} L_{kij}x_{kj} + z_s^2[f_k(x_{1i}x_{2i}) - \delta_{2k}\beta x_{2i}] = 0 \quad i=1,\ldots,M, \; k=1,2 \tag{42}$$

where

$$L_{kij} = \frac{B_{ij}}{Pe_k} - z_s A_{ij}$$

$$+ [(A_{00}-Pe_k z_s)(A_{M+1,M+1}-b_{k0}) - A_{M+1,0}A_{0,M+1}]^{-1}$$

$$\{[A_{0,M+1}(A_{M+1,j}-a_{k0}) - (A_{M+1,M+1}-b_{k0})A_{0j}](\frac{B_{i0}}{Pe_k}) - z_s A_{i0}$$

$$+ [A_{M+1,0}A_{0j}+(A_{00}+Pe_k z_s)(a_{k0}-A_{M+1,j})] (\frac{B_{i,M+1}}{Pe_k} - z_s A_{i,M+1})\} \qquad (43a)$$

with

$$a_{10} = b_{10} = 0 \qquad (43b)$$

$$a_{20} = b_{20} = 0 \qquad \text{for } \beta=0 \qquad (43c)$$

$$a_{20} = -x_{2w}b_{20} = x_{2w}z_s \frac{\alpha_2\alpha_1[e^{-\alpha_2(1-z_s)} - e^{-\alpha_1(1-z_s)}]}{\alpha_1 e^{-\alpha_2(1-z_s)} - \alpha_2 e^{-\alpha_i(1-z_s)}} \quad \text{for } \beta>0 \qquad (43d)$$

For a given set of parameters, B, Da, Pe_1, Pe_2, β, and γ these equations can be solved by Newton-Raphson's method and the spline point can be adjusted such that $x_{1,M+1} \doteq 1$ and wiggles are avoided.

In order for the method to handle cases where the reaction front is sharp and at the same time situated close to the outlet of the reactor, one or two additional collocation points may be needed. Such profiles, of which Figure 3 gives an example, arise when the Peclet numbers and the heat transfer are large. The steady state collocation equations are then:

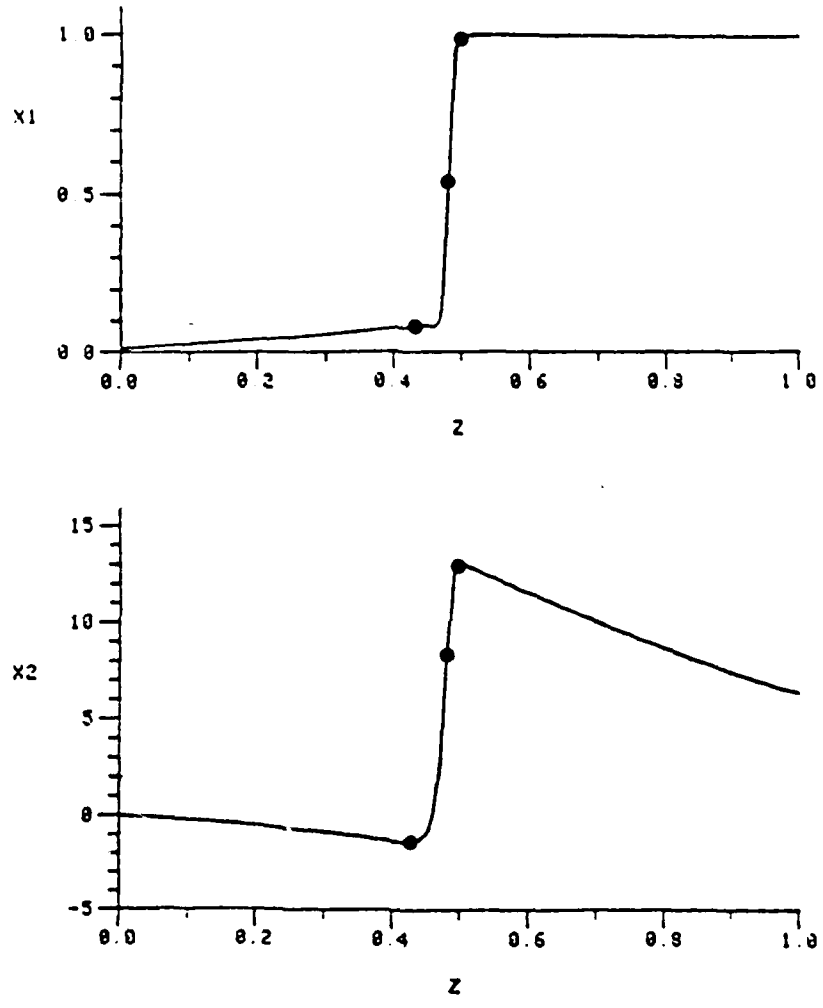

Figure 3 Example of a steady state profile for which three spline points (•) are necessary. B = 16.8, Da = 0.337, Pe_1 = 320, Pe_2 = 100, x_{2w} = -9.6, β = 0.72, γ = 16.9.

at the left hand boundary:

$$\sum_{j=0}^{M_1+1} A_{1ij} x_{kij} = \Delta z_1 x_{kij} \tag{44}$$

at the interior points of the ℓ'th element:

$$\sum_{j=0}^{M_\ell+1} \left[\frac{B_{\ell ij}}{Pe_k} - \Delta z_\ell A_{\ell ij}\right] x_{k\ell j} + \Delta z_\ell^2 \left[f_k(x_{1\ell i}, x_{2\ell i}) - \delta_{2k} \beta x_{2\ell i}\right] = 0 \tag{45}$$

$$i=1,\ldots,M \; ; \; \ell=1,\ldots,L$$

at each division between the spline intervals:

$$x_{k,\ell+1,1} = x_{k\ell,M+1} \tag{46a}$$

$$\frac{1}{\Delta z_\ell} \sum_{j=0}^{M_\ell+1} A_{\ell,M+1,j} x_{k\ell j} = \frac{1}{\Delta z_{\ell+1}} \sum_{j=0}^{M_{\ell+1}+1} A_{\ell+1,1j} x_{k,M+1,j}, \tag{46b}$$

$$\ell=1,\ldots,L-1$$

at the right hand boundary:

$$x_{kL}\Big|_{\zeta_L} = x_k\Big|_{z_s^+} \; ; \; k=1,2 \tag{47a}$$

$$\sum_{j=0}^{M_L+1} A_{L,M+1,j} x_{1Lj} = 0 \tag{47b}$$

$$\frac{1}{\Delta z_L}\sum_{j=0}^{M_L+1} A_{L,M+1,j}\,x_{2Lj} = \begin{cases} 0 & \text{for } \beta=0 \\ \dfrac{b_{20}}{z_s}\left(x_2\Big|_{z_s^+} - x_{2w}\right) & \text{for } \beta\neq 0 \end{cases} \tag{47c}$$

where

$$\zeta_\ell = \frac{z-z_{\ell-1}}{\Delta z_\ell}\ ;\ \Delta z_\ell = z_\ell - z_{\ell-1}\ ;\ z_0 = 0 \tag{48}$$

When the first of the additional spline points is placed at the inflection point of the temperature profile, very accurate results are obtained because then the energy balance is satisfied also at the spline point. The second point, which is seldom needed, should be placed at a local minimum of the temperature profile, if such a minimum exists in the interval $0<z<1$. Otherwise, accurate results are obtained if it is placed between the inlet and the inflection point of the temperature profile such that it halves the temperature rise between those locations.

In order to illustrate the ability of this spline collocation method to accurately predict very sharp profiles, we consider an example previously published by Lübeck [8], Figure 1] where the Peclet numbers are large (Pe_1 = 320, Pe_2 = 160) and consequently the profiles are very steep as illustrated in Figure 4. Figure 5 shows the hysteresis in the exit conversion and temperature

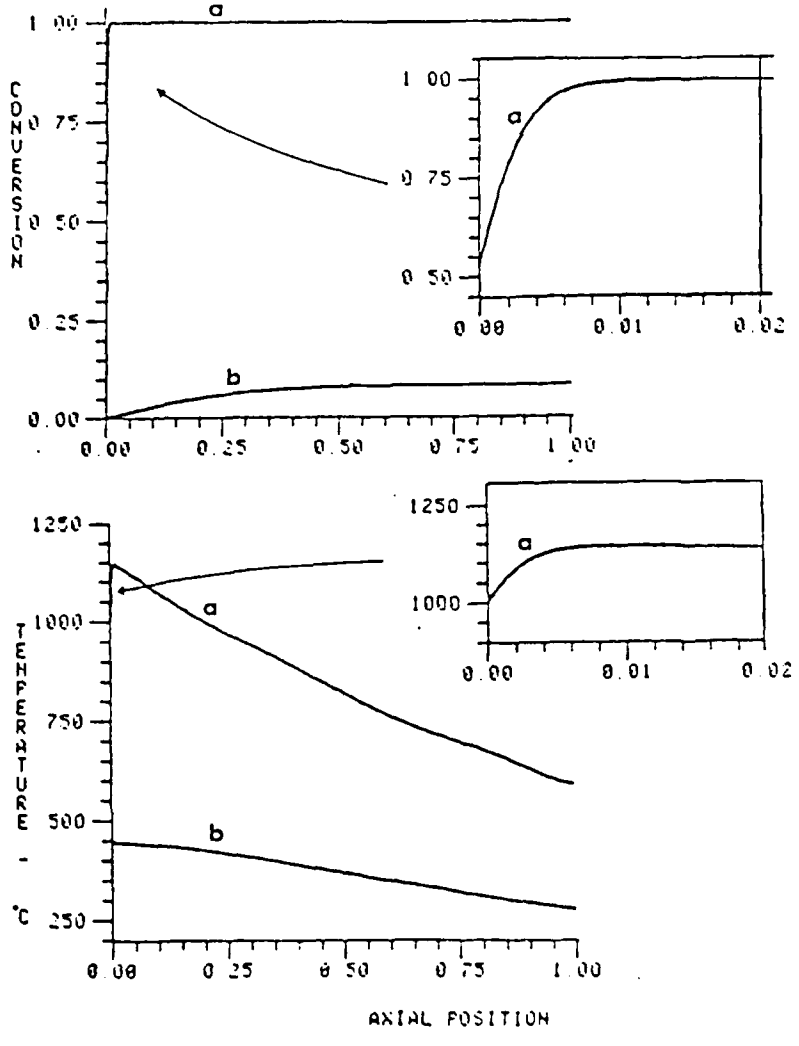

Figure 4 An example of steep conversion and temperature profiles found by spline collocation. (a) Upper steady state, (b) lower steady state. $B = 16.8$, $Da = 0.330$, $Pe_1 = 320$, $Pe_2 = 100$, $x_{2w} = 9.6$, $\beta = 0.72$, $\gamma = 16.9$.

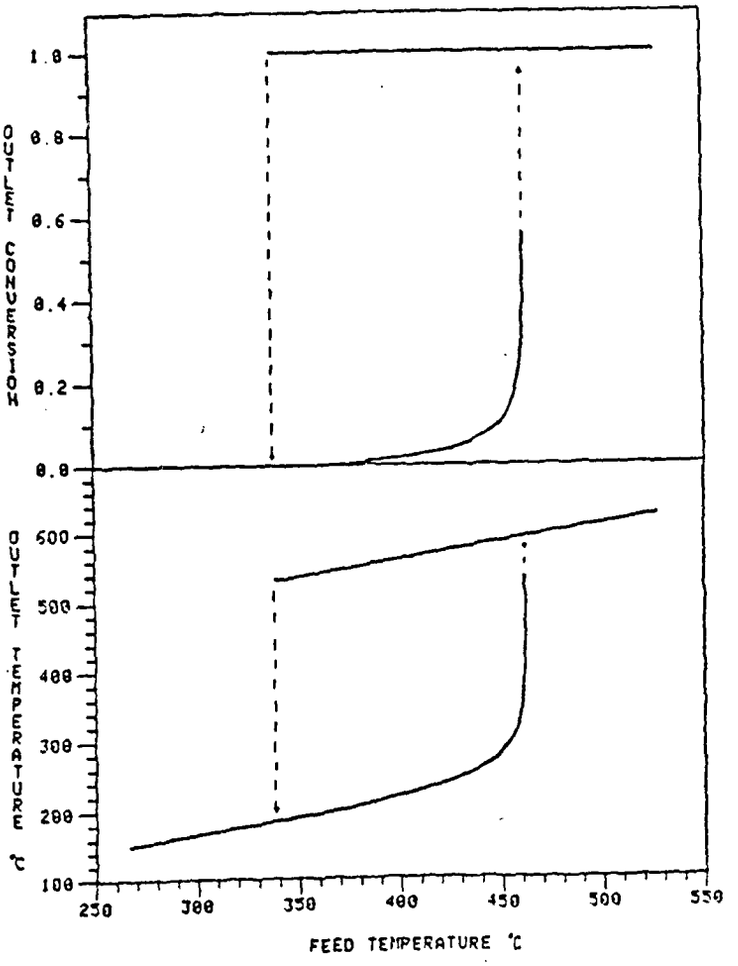

Figure 5 Ignition and extinction behavior of outlet conversion and temperature for Lübeck's example [89] . $Pe_1 = 320$, $Pe_2 = 100$, $\beta = 0.72$, $B = 8.7 \cdot 10^6 T_f^{-2}$, $Da = 7.33 \cdot 10^6 e^{-\hat{\gamma}}$, $\gamma = 1.22\ 10^4 T_f^{-1}$, $x_{2w} = \gamma(310-T)T_f^{-1}$, T_f feed temperature in °K.

as the feed temperature is changed. Lüleck simulated ignition when the feed temperature was increased from 459°C to 464°C and found extinction when the temperature was decreased from 355°C to 330°C. Our results are in agreement with those values; we find ignition and extinction when the feed temperature is 461.8°C and 339.2°C respectively.

The computations illustrated in Figures 3, 4, and 5 were based on three spline intervals (besides the dead-zone) with six collocation points in each. The two additional spline points were not really necessary in the calculation of the profiles shown in Figure 4, but they were required for the calculation of the intermediate and unstable profiles similar to the one shown in Figure 3.

5. STATIC BIFURCATION

Three methods are available in calculating the static bifurcation points. These are: (i) a direct approach entirely based on the steady state collocation equations, (ii) a more general extrapolation procedure based on finding zero eigenvalues of the Jacobian, Equation (17), and (iii) a turning point calculation based on the Newton-Euler Steady State algorithm.

(i) The direct approach. Here the bifurcation points are located by finding the parameter set for which the Jacobian of the steady state collocation equations becomes singular. The bifurcation point can only be approached from one side (in the case sketched in Figure 6 from the right hand side on the upper branch and from the left hand side on the lower branch), otherwise the Newton-Raphson iteration fails to converge or

converges to a different solution. Therefore, this method is not recommended.

(ii) A general extrapolation approach. The idea here is to linearize around a steady state point, (Da_s, $x_{1s}(z)$, $x_{2s}(z)$) away from the bifurcation point, Da_b^*, and then use the condition det ($\underset{\sim}{J}$) = 0 to successfully extrapolate to the bifurcation value of the parameter Da (cf. Figure 6). This requires additional computation in evaluating the necessary terms, N, in the Jacobian Equation (17). Figure 7 shows for various values of the Damköhler number used in the linearization, Da_s, the value of the predicted bifurcation point Da_b as functions of the number of terms, N, in the Galerkin expansion. Note that while there is movement toward the correct value of Da, iterative relinearization and prediction are required for convergence. However, this is plagued with singular problems because $Da_b > Da_b^*$ (cf Fig. 6). Expanding the dimension to include arc-length as Keller [90] suggests would be helpful, but we found the following method to be even more efficient.

(iii) Turning point calculations. Because the static bifurcation points in this problem and similar chemical reaction engineering problems, e.g. the catalyst particle problem, are turning points, one may use a very simple approach involving suitable change of dependent variables such that the system equations have a unique solution. This approach was taken by Sørensen et al. [91] who were able to trace out the solutions to the catalyst particle problem in the region of multiple steady states by using the value of the concentration at a collocation point as a parameter rather than the Thiele modulus itself. Here we also choose to fix a concentration and include

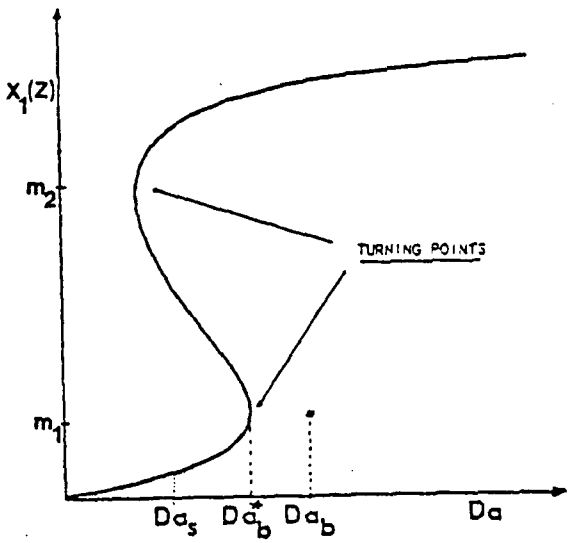

Figure 6 Steady state value of $x_1(z)$ for varying Da. The curve has two turning points, m_1 and m_2.

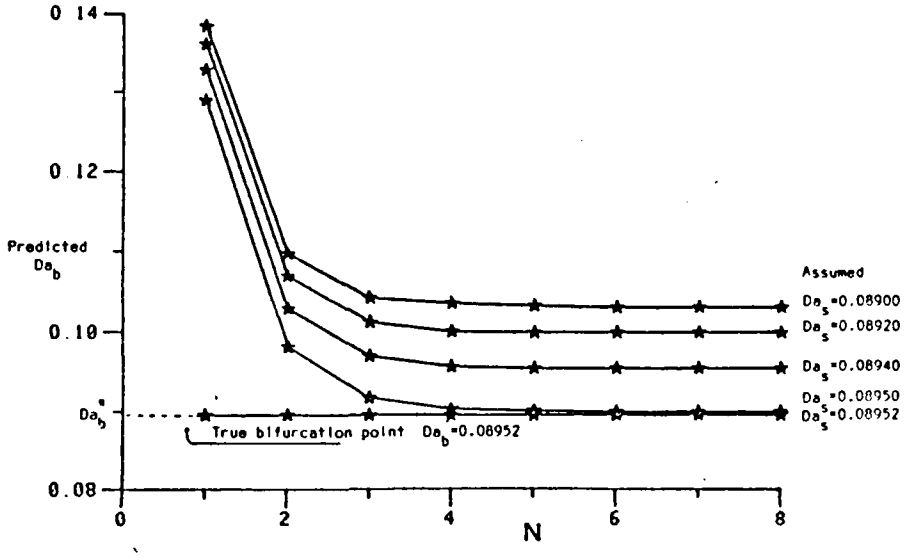

Figure 7 The predicted bifurcation points, Da_b, for various assumed values, Da_s, and varying number of terms, N, in the Galerkin expansion.

the Damköhler number as a dependent variable. In the adiabatic case it can be shown that the profiles cannot intersect [92], so the parameter change renders a set of equations which have a unique solution. However, in the nonadiabatic case, both the concentration and temperature profiles can intersect [45, Figure 11]. Extensive calculations [e.g. 40,44,45,93] indicate, as is physically expected, that for constant B, Pe_1, Pe_2, β, and γ at the exit of the reactor

$$\left.\frac{dx_1}{dDa}\right|_{z=1} \neq 0 \tag{49}$$

Therefore, we may choose the exit concentration as a parameter so that the collocation equations become:

$$\sum_{i=1}^{M+1} L_{1ij}x_{ij} + z_s^2 f_1(x_{1i},x_{2i}) = 0 \qquad i=1,\ldots,M \tag{50}$$

$$\sum_{i=1}^{M+1} A^*_{M+1,j}x_{ij} = 0 \tag{51}$$

$$\sum_{i=1}^{M} L_{2ij}x_{2j} + z_s^2[f_2(x_{1i},x_{2i}) - \beta x_{2i}] = 0 \quad i=1,\ldots,M \tag{52}$$

where Da is a dependent variable. The boundary condition at $z = 0$ is now included so $A^*_{M+1,j}$ and L_{1ij} take the form:

$$A^*_{M+1,j} = A_{M+1,j} - (A_{00} - Pe_1 z_s)^{-1} A_{M+1,0}A_{0j} \tag{53a}$$

$$L_{1ij} = \frac{B_{ij}}{Pe_1} - z_s A_{ij} - (A_{00} - Pe_1 z_s)^{-1} A_{0j} \left(\frac{B_{i0}}{Pe_1} - z_s A_{i0} \right) \tag{53b}$$

while L_{2ij} is still defined by (43a).

This set of nonlinear algebraic equations can be solved by the Newton-Raphson procedure, provided a sufficiently good initial guess is available. This initial guess can be determined as follows. We differentiate the equations with respect to $x_{1,M+1}$ to determine the sensitivity of x_{1j}, x_{2j}, Da to a step in outlet conversion $x_{1,M+1}$.

$$\sum_{J=1}^{M} L_{1ij} \frac{\partial x_{1j}}{\partial x_{1,M+1}} + z_s^2 \left[\frac{\partial f_1}{\partial x_{1i}} \frac{\partial x_{1i}}{\partial x_{1,M+1}} + \frac{\partial f_1}{\partial z_{2i}} \frac{\partial x_{2i}}{\partial x_{1,M+1}} + \frac{\partial f_1}{\partial Da} \frac{\partial Da}{\partial x_{1,M+1}} \right] = - L_{1i,M+1}, \qquad i=1,\ldots,M \tag{54}$$

$$\sum_{J=1}^{M} A^{*}_{M+L,j} \frac{\partial x_{1j}}{\partial x_{1,M+1}} = - A^{*}_{M+1,M+1} \tag{55}$$

$$\sum_{j=1}^{M} L_{2ij} \frac{\partial x_{2i}}{\partial x_{1,M+1}} + z_s^2 \left[\frac{\partial f_2}{\partial x_{1i}} \frac{\partial x_{1i}}{\partial x_{1,M+1}} + \left(\frac{\partial f_2}{\partial x_{2i}} - \beta \right) \frac{\partial x_{2i}}{\partial x_{1,M+1}} + \frac{\partial f_2}{\partial Da} \frac{\partial Da}{\partial x_{1,M+1}} \right] = 0 \qquad i=1,\ldots,M \tag{56}$$

This system of linear equations can be solved for a step in outlet conversion $x_{1,M+1}$ to yield the next initial guess for Eqns. (50-52).

For the first step, one may begin from the known trivial solution to the steady state equations:

$$Da = 0:$$

$$x_{1j} = 0$$

$$x_{2j} = 0 \qquad \text{if } \beta=0$$

$$x_{2j} = x_{2w}\left[1-Pe_2\frac{\alpha_1 e^{-\alpha_2(1-z_j)} - \alpha_2 e^{-\alpha_1(1-z_j)}}{\alpha_1^2 e^{-\alpha_2} - \alpha_2^2 e^{-\alpha_1}}\right] \tag{57}$$

$$j = 0,1,\ldots,M+1$$

The system of equations (50-52) and (54-56) form a Newton-Euler algorithm, where they respectively function as corrector and predictor. Because the left hand of the Newton-Raphson correction solution to Equations (50-52) is the same as the left hand side of Equations (54-56), the inverse of the Jacobian needed for the Euler prediction step is already available (if for example the LU decomposition is used). Thus the prediction step, equations (54-56), requires only an inexpensive back substitution. The above formulae have been based on the simple collocation method, but two additional spline points can readily be included as was done above in Equations (44-48). The Newton-Euler algorithm is used throughout the following bifurcation studies.

In order to check this static bifurcation algorithm we considered two previously published calculations. Using the spline collocation procedure described above, we calculated the bifurcation curves shown in Fig. 2b. These are in good agreement with the results of Hlaváček and Hofmann [38b, Fig. 15] except for a very slight difference in the value of the Peclet number at the trifurcation point (i.e. the confluence of the bifurcation curves). We obtain Pe = 31.88 whereas Hlaváček and Hofmann report a value of Pe = 31.05.
The second example is taken to be a case with five steady states studied earlier [93, Table 2]. Our procedure gives the same values for Da at bifurcation as the GPM-technique of Kubíček and Hlaváček [93]. This example assumed $\gamma \to \infty$. It is interesting to note that for the same parameters and rather large, finite γ ($\gamma \tilde{=} 100$), further calculations show that only three steady states are possible (in agreement with recent results of Kapila et al. [46]).

6. HOPF BIFURCATION

Two basic approaches exist for evaluating the Hopf bifurcation points: (i) direct methods based on actual computations of the eigenvalues or (ii) indirect procedures based on the magnitudes of the coefficients of the characteristic polynomial. In the first method all the eigenvalues are calculated, preferably by a QR algorithm, (cf. [94] for the original description and [81, p. 421] for an efficient FORTRAN routine) and the most positive real part of the complex eigenvalues is chosen as a residual. This is then made as close to zero as is wanted by varying the bifurcation parameter [95]. Clearly, the search is abandoned

if the real part of any of the other eigenvalues is positive.
(ii) In the indirect methods the Hopf bifurcation points are determined by varying the parameters to satisfy necessary conditions formulated in terms of the coefficients of the characteristic polynomial:

$$P(\lambda) = \lambda^{2N} - S_1\lambda^{2N-1} + S_2\lambda^{2N-2} - \cdots + S_{2N-2}\lambda^2 - S_{2N-1}\lambda + S_{2N} = 0 \quad (58)$$

Here N is the number of terms in the collocation or Galerkin approximation and the coefficients, S_i, are the sums of the principal minors of the Jacobian Equation (17), [96, ct. 4]. Necessary conditions that the characteristic polynomial has two purely imaginary roots:

$$\lambda_{1,2} = \pm i\sqrt{\omega} \qquad \omega > 0 \quad (59)$$

are:

$$(-1)^N\omega^N + (-1)^{N-1}S_2\omega^{N-1} + \cdots + (-1)S_{2N-2}\omega + S_{2N} = 0 \quad (60)$$

and

$$(-1)^{N-1}S_1\omega^{N-1} + (-1)^{N-2}S_3\omega^{N-2} + \cdots + (-1)S_{2N-3}\omega + S_{2N-1} = 0 \quad (61)$$

In order to have bifurcation we must further have an exchange of stability. The stability test is conveniently made using the Routh-Hurwitz criterion as well as the necessary condition that the coefficients $(-1)^{2N-i}S_i$ must be positive.

For $N = 1$ and $N = 2$ the necessary conditions for Hopf bifurcation may be reduced to:

for N=1

$$S_1 = 0 \quad (62a)$$

$$S_2 > 0 \quad (62b)$$

for N=2

$$\frac{S_3}{S_1}\left(\frac{S_3}{S_1} - S_2\right) + S_4 = 0 \tag{63a}$$

$$S_1 < 0 \tag{63b}$$

$$S_3 < 0 \tag{63c}$$

$$S_4 > 0 \tag{63d}$$

Recently, Kubíček [97] presented two variants of the above procedure where he combined the Hopf conditions and steady state equations and solved the entire system by Newton-Raphson iteration. However, such a procedure is likely to cause difficulties in the present tubular reactor problem because of the large search space combined with local convergence of Newton's method. Instead we use the Newton-Euler steady state algorithm and search over Da for a solution to equations (60) and (61) in the parameter region where the necessary condition, $(-1)^{2N-i}S_i > 0$, is satisfied. When a solution has been found, we use the Routh-Hurwitz criterion to check the sign of the real part of the remaining eigenvalues. This approach works well for $N \leq 2$, whereas for larger N the direct approach (i) gives faster and more accurate results.

The direction and stability of the bifurcating orbits can be determined, in principle, by applying the standard formulae for ODEs [70,98] to the collocation or Galerkin approximations (cf. Section 3) since these represent $F_{\underset{\sim}{x}}$ correctly in the limit of large N. Alternatively one may use the new formula

of Heinemann and Poore [99]. However, the stability of periodic solutions is not pursued in detail here.

At the time these Hopf bifurcation algorithms were developed, no calculations of Hopf bifurcation points in tubular reactor equations had been carried out to our knowledge. Therefore, we had to be satisfied with comparing the parameter values at bifurcation points with those used in simulations of limit cycles. For example, Hlaváček and Hofmann [39] found a stable limit cycle for the parameters $B = 11.0$, $Pe_1 = Pe_2 = 1.0$, $Le = 1.0$, $x_{2w} = 0.0$, $\beta = 2.0$, $Da = 0.200$ and $\gamma \to \infty$. This compares well with our result that stable limit cycles should exist at least between the two Hopf bifurcation points, $Da = 0.153$ and $Da = 0.238$.

In addition, the forthcoming paper by Heinemann and Poore [99] offers an aposteriori check of our algorithms, since they have calculated the Hopf bifurcation points corresponding to the original simulations of Varma and Amundson [45b]. Application of our algorithm gave the same results as obtained by Heinemann and Poore [99] for these examples [37].

The convergence properties of the Galerkin and collocation procedures were studied in general by varying the number of terms in the evaluation of the critical Lewis number, Le_c. This number represents the maximum value of the Lewis number that allows Hopf bifurcation and thus gives a good measure of the convergence properties of the above algorithms. The actual calculation of Le_c is detailed below. As also found by McGowin and Perlmutter [53], we show that the Galerkin procedure converges monotonically while the collocation method converges in a dampened oscillatory

[illegible]

[illegible]

We are now able to describe the possible steady state and dynamic behavior for a single first order reaction in a tubular reactor with axial dispersion as a function of the values of the parameters. Because the reactor behaves like a CSTR in the limit of small Peclet numbers, we use the detailed description of the dynamic behavior of the CSTR, given by Uppal et al. [6], as a starting point and show how the bifurcation structure of the dispersion model changes as the value of the Peclet number increases. Figure [illegible] illustrates the various regimes of the dynamic behavior of the CSTR in the B-β-parameter space. For parameter combinations above the curve M_1, static bifurcation, i.e., branching to multiple steady states, occurs at two values of the bifurcation parameter, Da. Hopf-bifurcation, i.e., branching to periodic solutions, is possible for values of (B,β) above the curves S_1 and S_2. In the region between the S_1 and S_2 curves there are two Hopf-bifurcation points, while only one point exists in the region above S_1. The curves M_1, S_1, and S_2 form six regions whose bifurcation behavior are illustrated by the

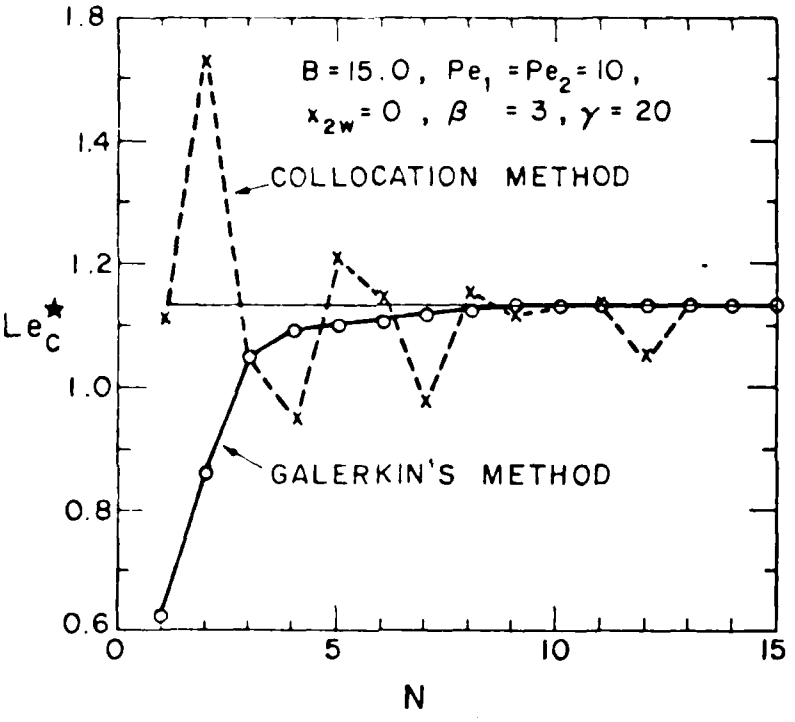

Figure 8 The critical Lewis number, Le_c^*, for varying number of terms, N, in the collocation procedure (x) and in Galerkin's method (o).

peripheral sketches in Figure 9. Uppal et al. [66] also give the direction and stability of the bifurcating orbits as well as phase portraits of the possible dynamic behavior. However, similar results for the tubular reactor are not included here, because classifying the stability of periodic solutions is beyond the scope of the present study.

The B-β parameter space plot, illustrated in Figure 10, shows the various regimes of bifurcation behavior for the axial dispersion model with $Pe_1 = Pe_2 = 5$. This diagram was calculated using the Newton-Euler steady state algorithm with 2 spline points and 6-10 collocation points in each element. The eigenvalue calculations were based on Galerkin's method with the first 6 eigenfunctions.

In addition to the M_1, S_1, and S_2 curves also found in the CSTR case, there is a multiplicity curve, M_2 and Hopf-bifurcation curves S_3', S_3'', and S_4. The curve M_2 represents the appearance of a second set of static bifurcation points not found in the CSTR. Note that for large β, these may occur for lower values of B than the first set (which arise above M_1). Thus the tubular reactor may more easily show multiplicity than the CSTR for large amounts of cooling. The curves S_3', S_3'' allow additional Hopf bifurcation points to appear as β increases, while curve S_4 marks the simultaneous disappearance of two Hopf bifurcation points by coalescence. These M and S curves divide the parameter space into 14 regions, I-XIV; the first 6 of which, i.e., I-VI, are the same as those found in the CSTR analysis (cf. Figure 9) whereas the others are new. The bifurcation behavior

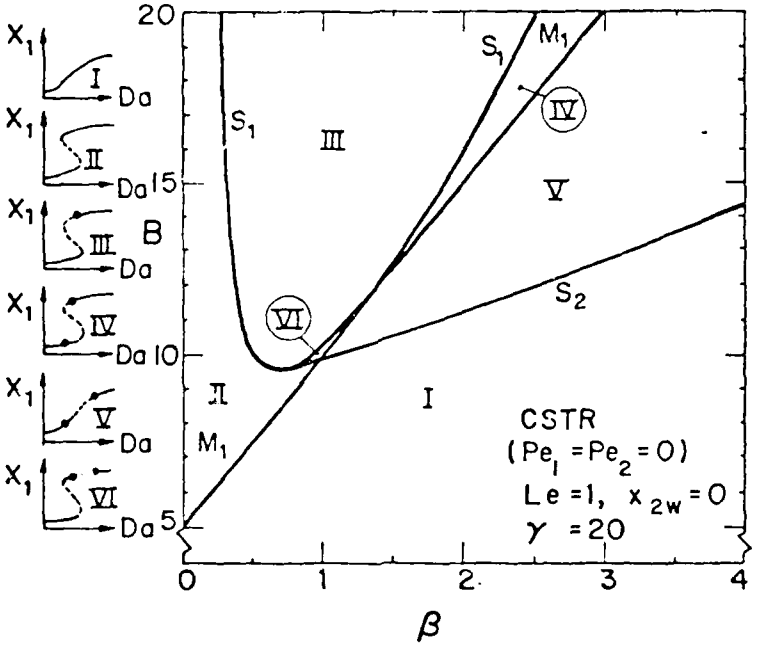

Figure 9 Classification of the dynamic behavior of the CSTR in the parameter space B-β [66].

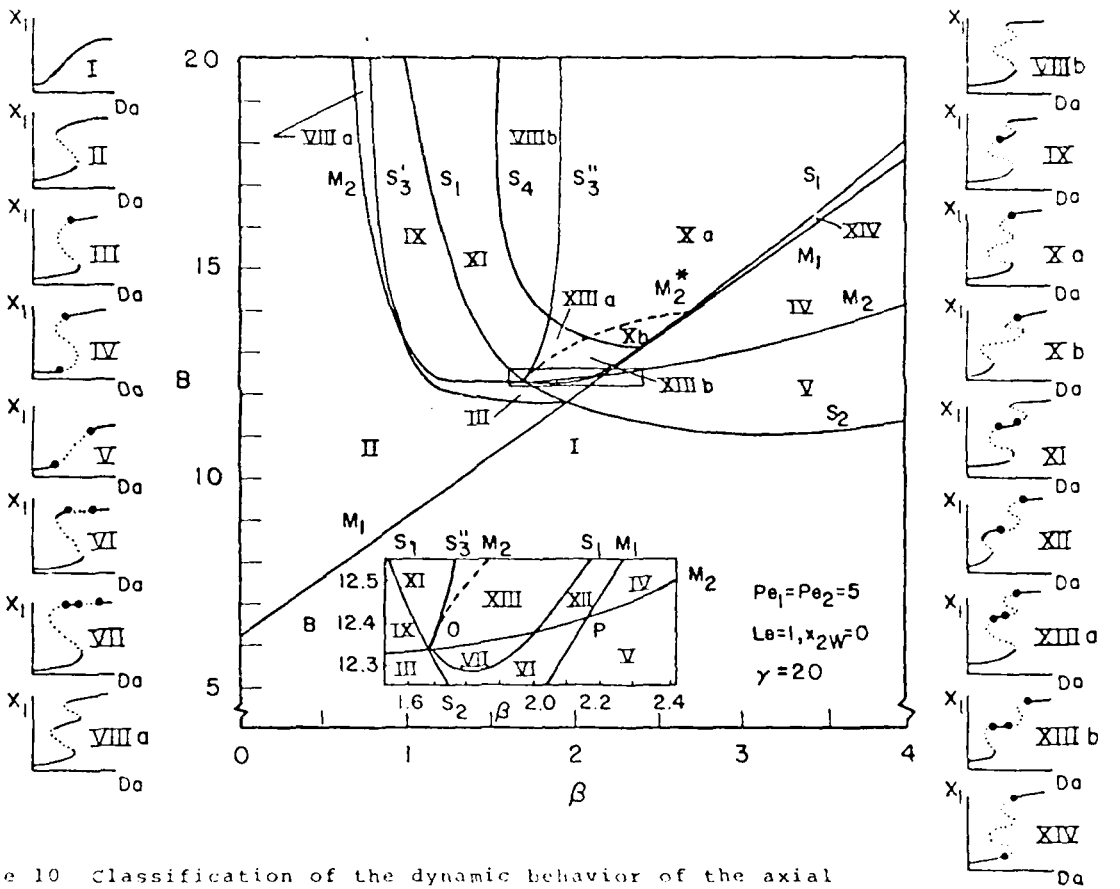

Figure 10 Classification of the dynamic behavior of the axial dispersion model (Pe = 5) in the parameter space B-β. In the peripheral figures: —— stable state, ---- unstable state, ● Hopf bifurcation points.

expected in each region is illustrated by the sketches of the variation of the steady state exit conversion, x_1, with the bifurcation parameter, Da. Specific numerical simulations of changes in the steady state exit conversion, x_1, and temperature, x_2, with Da are shown in Figure 12a-r and the corresponding values of B and β are summarized in Table 2 and Figure 11. The vertical lines in Figures 12b,d,i and q indicate the values of Da for which the steady state profiles are shown in Figure 13. The bifurcation structure is detailed in the following paragraphs.

The two multiplicity curves, M_1 and M_2, intersect at the point P, $(B,\beta) \doteq (12.4, 2.2)$ (cf. Figure 10). For parameter combinations to the left of P, above M_1 and below M_2, x_1 versus Da has two turning points, m_2, m_1, i.e., three steady state profiles exist for a range of Damköhler numbers (cf. Figure 12b). Figure 13(i) gives an example of such multiple steady state profiles. If (B,β) moves above M_1 and M_2, a second set of static bifurcation points, m_4, m_3, appear in the x_1, x_2 curves. In this case five steady states are possible if the two sets of multiplicities overlap, i.e., $Da(m_4) \leq Da(m_1)$ (cf. Figure 12i); otherwise there are two regions of three steady states as illustrated in Figure 12p. The broken curve M_2^* represents the parameter combinations, (B,β) for which $Da(m_1) = Da(m_4)$ and thus separates the regions where the two phenomena occur. M_2^* is <u>not</u> a bifurcation boundary but it is interesting to note that ' comes very close to the point O where the M_2, S_1, S_2, and curves intersect (cf. Figure 10).

To the right of the intersection of M_1 and M_2, (point P),

Table 2 Summary of numerical simulations

Case	Region	B	β	Figure
a	I	11.0	2.25	12a
b*	II	11.0	1.50	b
c	III	12.0	1.50	c
d*	IV	14.0	3.00	d
e	V	12.0	2.25	e
f	VI	12.0	1.95	f
g	VII	12.3	1.80	g
h	VIIIa	18.0	0.75	h
i*	VIIIb	15.5	1.75	i
j	IX	12.6	1.50	j
k	Xa	15.5	3.00	k
l	Xb	13.3	2.25	l
m	XI	14.0	1.50	m
n	XII	12.6	2.25	n
o	XIIIa	13.3	1.95	o
p	XIIIb	12.4	1.75	p
q*	XIIIc	13.0	2.25	q
r	XIV	17.8	4.00	r

*Steady profiles calculated for fixed Da, cf. Figure 13.

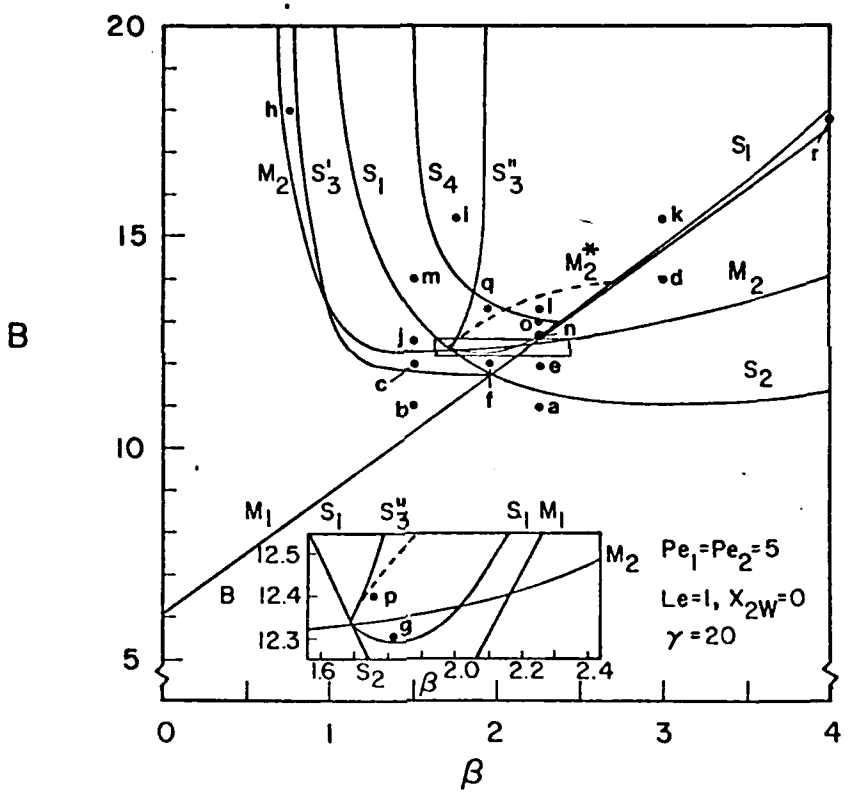

Figure 11 Classification of the dynamic behavior of the axial dispersion model (Pe = 5) in the parameter space B-β. Cf. Figure 12a-r and Table 2 for further details.

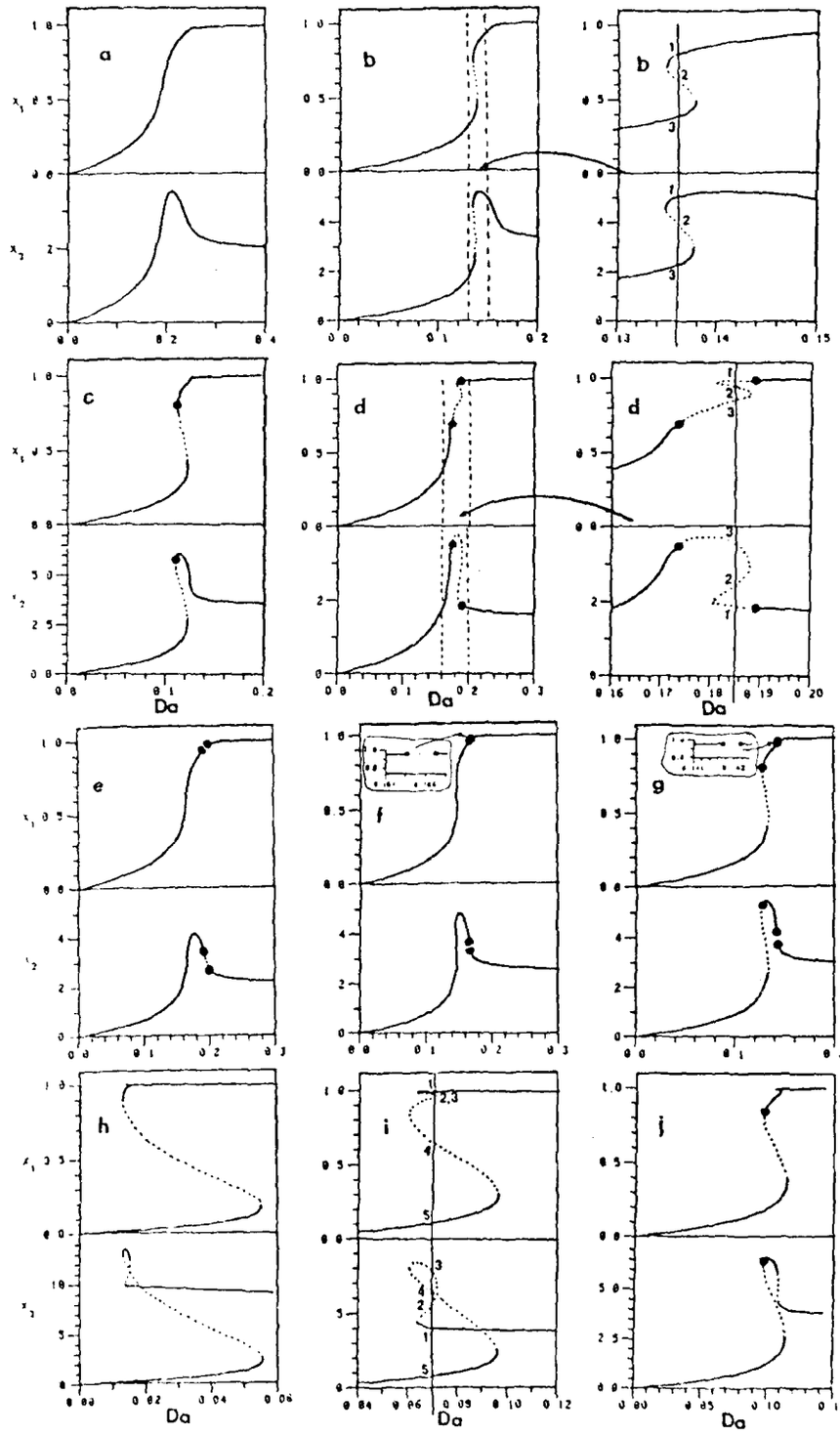
a
b
b
c
d
d
e
f
g
h
i
j
Da
Da
Da
Da

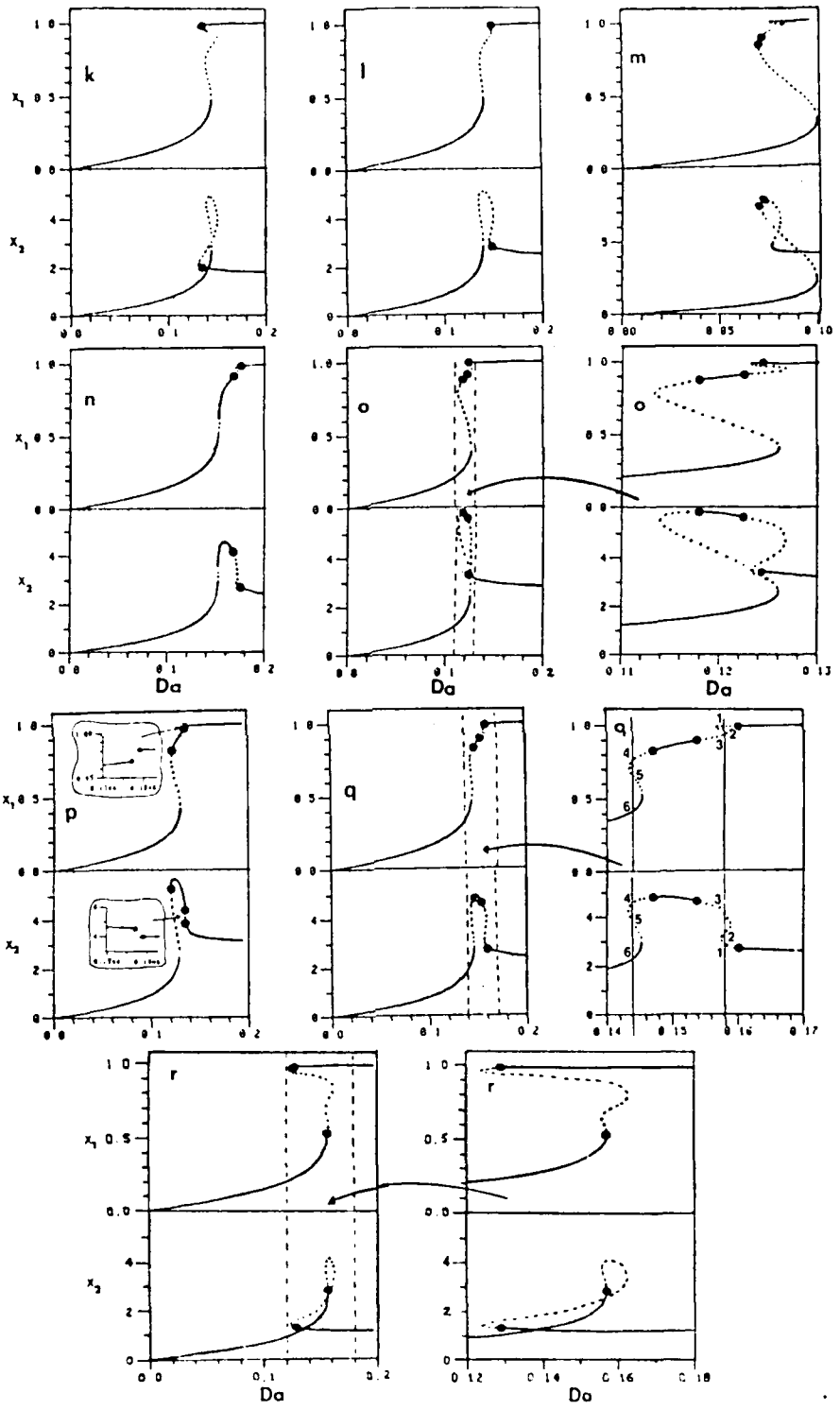

Fig. 12 (Continued)

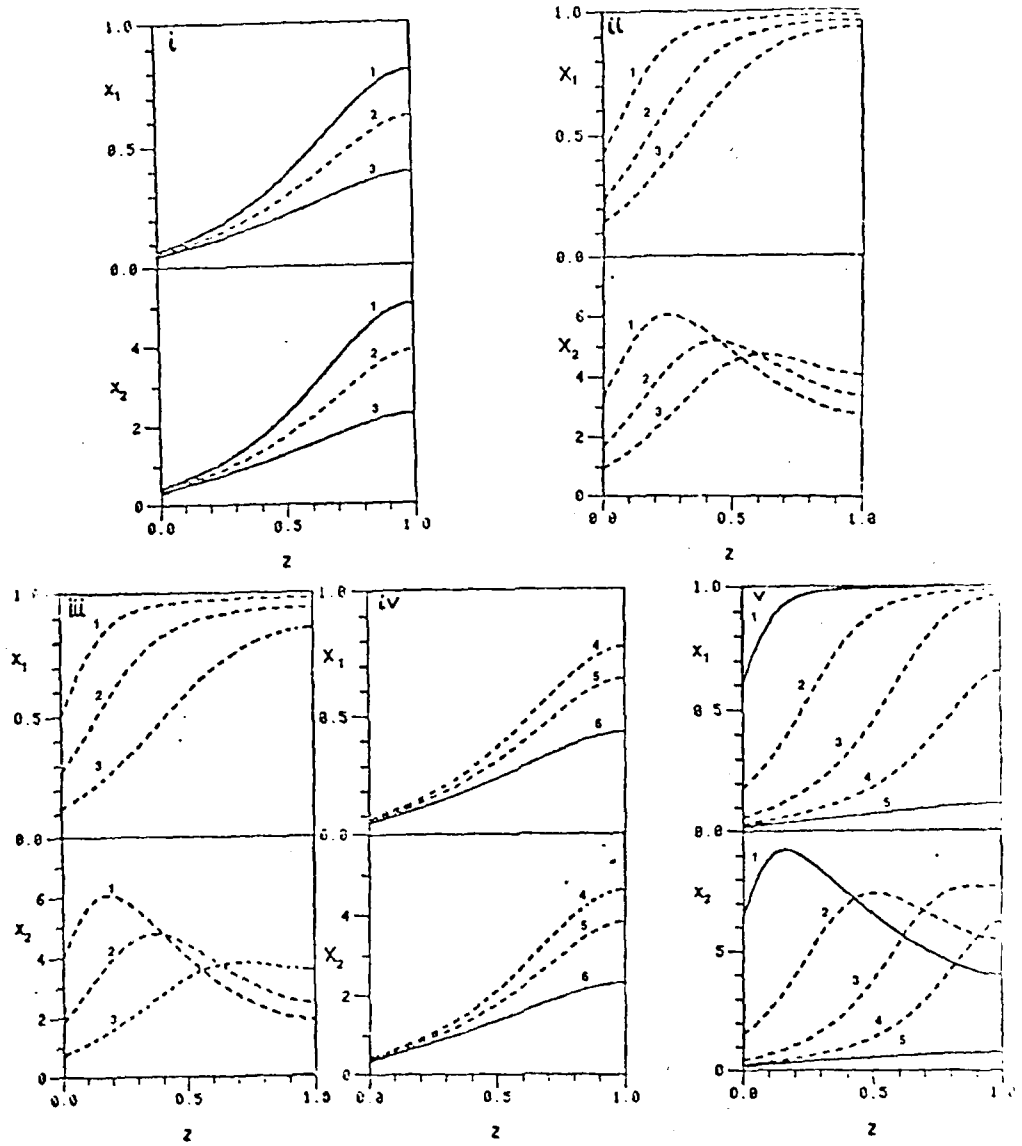

Figure 13 Steady state profiles; —— stable, --- unstable

(i) case b Table 5 (Region II); Da = 0.136
(ii) case d Table 5 (Region IV); Da = 0.185
(iii) case q Table 5 (Region XIIIb); Da = 0.144
(iv) case q Table 5 (Region XIIIb); Da = 0.158
(v) case i Table 5 (Region VIIIb); Da = 0.070

three steady states are possible for (B,β) in the region below M_1 and above M_2. Thus the turning points are: m_3 and m_4, and the multiplicity occurs at higher conversions than is the case for parameters to the left of P. Furthermore, the multiplicity now occurs to the right of the maximum in the x_2 curve (compare Figures 12b and d). As illustrated by Figure 13(ii) the steady state temperature profile now has a maximum inside the reactor because of the increased heat transfer (β). This maximum moves forward and becomes more pronounced as the reaction ignites. A second set of turning points, m_1 and m_2, appears when (B,β) rises above M_1 and then the multiplicity pattern is again either 1-3-1-3-1 (cf. Figure 12q) or 1-3-5-3-1 (cf. Figure 12k). In the very special cases where $Da(m_1) = Da(m_3)$ or $Da(m_2) = Da(m_4)$ the patterns become 1-3-5-1 or 1-5-3-1, respectively. Clearly, if (B,β) pass through the point, P, m_1, m_2, m_3, and m_4 appear simultaneously so that one goes from a region with a unique steady state (cf. Figure 12a) to a region where three steady states exist over two disjoint intervals of Damköhler numbers (cf. Figure 12n). Figures 13iii and 13iv give respectively, examples of steady state profiles for cases with 1-3-1-3-1 and 1-3-5-3-1 multiplicity. As expected, these profiles combine the characteristics of the ones in Figures 13(i) and 13(ii).

The Hopf-bifurcation structure is conveniently demonstrated by considering the different phenomena that comes about as either B or β is varied. First let us vary B keeping $\beta = 1.5$. In region I we have a unique globally stable steady state profile. As discussed above, two turning points exist

in region II (cf. Figure 12b). If B is increased past the S_3' curve into region III a Hopf bifurcation point, s_1, slides onto the upper branch (cf. Figure 12c). Above M_2, in region IX, the turning points, m_3, m_4, appear to the right of the Hopf point and therefore do not interfere with it (cf. Figure 12j). At the S_1 curve a second Hopf point, s_2, materializes on the middle branch (region XI, cf. Figure 12m); this time it comes in from m_3.

Since region XI extends to the upper boundary of the parameter space plot, we now hold B constant at some value above the intersection of S_3'' and S_4, say 15.5, and change β. As β is increased the Hopf points s_1 and s_2 approach each other and at S_4 they coalesce and disappear. This means that in region VIIIb the middle branch is unstable contrary to the case in region VIIIa (compare Figures 12h and 12i). Further increases in β bring us past S_3'' where a new Hopf bifurcation point comes onto the upper branch from m_4 (cf. Figure 12k). Then, β passes into region XIV through S_1 where a Hopf bifurcation point moves past m_1 down onto the lower branch (cf. Figure 12r). Note that region XIV is extremely small for $\beta < 4$. Finally increasing β leads one to region IV through M_1, where m_1 and m_2 coalesce and disappear. Figure 12d exemplifies the structure.

Next let us fix B at some value below the intersection of S_3'' and S_4 but above M_2 and vary β again starting in region XI. Now S_3'' is reached before S_4 so we enter region XIII where the Hopf point, s_3, appears on the upper branch while s_1 and s_2 still exist on the middle branch (cf.

Figures 12o-q). A further increase in β brings us into either region X by crossing S_4 (cf. Figure 12k,l) or region XII by crossing S_1 (cf. Figure 12n) depending on the value of B. In the first case, S_4' is encountered and s_1 and s_2 coalesce while in the second case s_2 moves past m_2 at curve S_1. From region X, increasing β leads us across S_1 into region XIV and across M_1 to region IV as before, while from region XII we enter region IV directly. If M_2 is passed, the multiplicity vanishes and region V appears (cf. Figure 12e).

Below the M_2 curve the S_2 curve forms the border between regions III and VI where a second Hopf point s_2 appears on the upper branch (cf. Figure 12f). If B is increased in region VI, either S_1 or M_1 is crossed. In the first case (region VII) a third Hopf point slides onto the upper branch from m_2 (cf. Figure 12g), while in the latter case (region XII) a multiplicity is formed between the two Hopf points (cf. Figure 12n). Increasing B in either region leads to region XIII.

Let us discuss the intersections between the M and S curves. Because the curves S_1 and S_3'' respectively represent parameter combinations where Hopf bifurcation points appear from under the turning points m_3 and m_4, the curves have to come together at the point O where S_1 crosses M_2. Also S_2 has to join at this point in order to preserve the balance of Hopf points. Similarly S_2 and S_3' have to coincide where S_2 intersects M_1 since they represent points which come onto the upper branch through the turning point m_2. Note that S_1 and M_1 "kiss" and depart again as in the case of the CSTR.

A rigorous analysis of the direction and stability of the branching periodic solutions has yet to be made in order to obtain the complete phase plane structures of each region. In addition to the nine basic phase portraits given by Uppal et al. ([66], Figure 6) one clearly would obtain new phase plots in the regions where five steady profiles and/or three Hopf bifurcations exist. However, the structure of these will not be entirely new, but rather combinations of characteristics of the basic plots. For example, the phase portraits of region XIII will be a combination of those for regions III and IV. Similarly, the plots for regions IX and X are likely to be a mixture for regions II and III. Because a unique unstable state is surrounded by a stable limit cycle, one knows without further analysis that stable limit cycles exist in regions IV-VII and XII-XIV. The original simulations by Varma and Amundson [45b, Figures 2.3 and 2.4] nicely illustrate with phase portraits and reactor profiles some of the possible limit cycle behavior in these regions.

Effect of Varying Peclet Number

As already demonstrated above, the most dramatic influence of the Peclet number on multiplicity and oscillatory phenomena is the introduction of an additional set of Hopf and static bifurcation points to augment those found for the CSTR. However, it is also rather interesting to consider the effect of the Peclet number on the critical values of B and β. Let us begin with the multiplicity limits and compare these exact limits with those predicted by Hlaváček's "linearization" [38] and the one point collocation method. Both these early lumping techniques give the following algebraic steady state equations:

[illegible]

(66a)

$$\tan\sqrt{[illegible]} \quad [illegible] \qquad (66b)$$

while in the one point collocation one has

$$\mu_i = \frac{2+Pe_i}{2+\frac{3}{4}Pe_i} \qquad i = 1,2 \qquad (67)$$

when Legendre polynomials are used as trial functions. The collocation point is then $z = 1/2$.

By solving for Da and finding the parameter sets for which $\frac{dDa}{dx_1} = 0$ is possible, one derives the necessary condition for multiplicity:

$$B > \frac{4(\mu_2+\beta+\beta x_{2w} [illegible])^2}{\mu_1[\mu_2+\beta-4/\gamma(\mu_2+\beta+\beta x_{2w} [illegible])]} \qquad (68)$$

Because both $\mu_i \to 1$ as $Pe_i \to 0$, this condition (68) approaches the usual one for the CSTR [66, inequality (12)] in the limit of small Peclet numbers, as it should. However, for large Peclet numbers, the criterion (68) takes different forms because as Peclet number becomes large, $\mu_i \to Pe_i$, while for Hlaváček's approximation $\mu_i \longrightarrow 4/3$ for the one point collocation approximation.

Figure 14 gives a comparison of the exact multiplicity

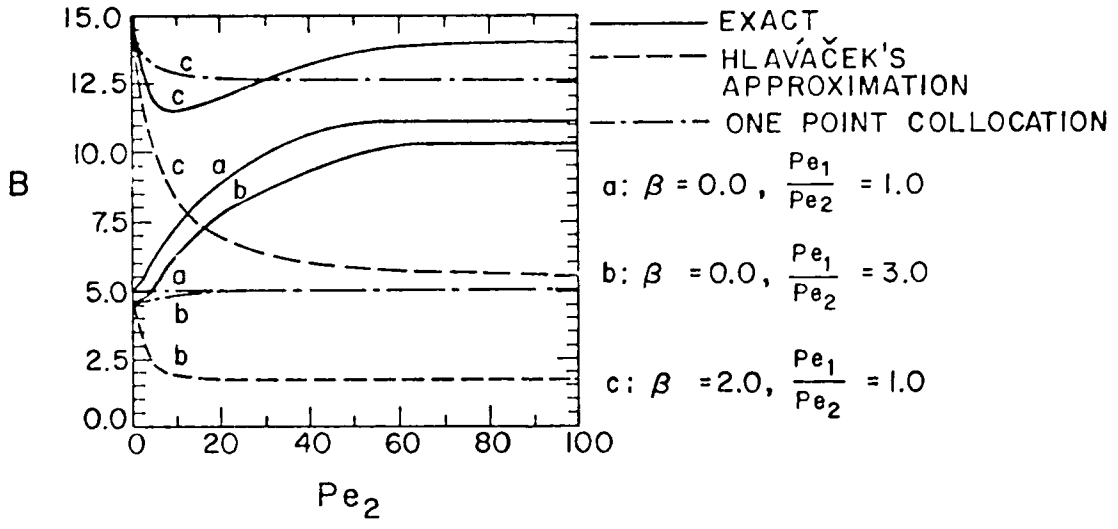

Figure 14 Comparison of exact and approximate limits of multiplicity.

[illegible] predicted by our algorithm and those predicted by the [illegible]. In the adiabatic case with equal [illegible] (curve a), the exact limit increases monotonically from the CSTR limit, $B_{crit} = 5$, while the predictions of lumping methods are independent of the value of the Peclet number. In the adiabatic case where $Pe_1 = 3Pe_2$ (curve b), as is typical for fixed bed reactors, the curve initially dips below the CSTR limit and then increases almost parallel to the curve (a). For this case Hlaváček's approximation decreases monotonically whereas the one point collocation method correctly predicts the dip but then straightens out at the CSTR condition. In the nonadiabatic case with $\beta = 2.0$ (curve c), the curve dips down and stays below the condition for multiplicity in the CSTR case, $B_{crit} < 11$. The lowering of the limit is due to two factors: 1. the new M_2 curve intersecting the M_1 line (cf. Figure 10), and 2) increasing slopes of the M_1 lines with increasing Peclet number. Although it has not been formally proven, our numerical calculations infer that the M_1 curves are also straight lines for $Pe > 0$. Whereas Hlaváček's approximation approaches the adiabatic CSTR condition asymptotically, the one point collocation prediction stays close to the exact limit. In fact for $Pe < 30$, it is above the exact limit and thus predicts uniqueness where there are multiple steady states. Although Hlaváček's approximation gives conservative multiplicity limits for the cases here, Varma and Amundson [45a] have shown that it, too, can falsely predict uniqueness. The fact that the exact boundaries flatten out shows that

multiplicity can occur even for large values of the Peclet numbers, i.e., in long reactors. However, as also demonstrated by Hlaváček and coworkers (e.g., [38b,43], the region of multiplicity can be very small at high Peclet numbers.

As illustrated in Figure 15, the region in the parameter space where limit cycles are possible diminishes as the Peclet number increases. Nevertheless, for $Pe < 10$ and large values of β, the critical value of B is lower than in the CSTR case, similar to the situation for the multiplicity limits. The maximum value of Pe for which oscillations exist for parameter combinations of practical interest (e.g.; $B \leq 20$, $\beta \leq 4$) may be inferred from our observation that no Hopf bifurcation points were found for $Pe = 15$, $B < 20$, and $\beta = 3.5$. Thus, oscillations due to the interaction of mixing and reaction processes occur only in very short reactors.

Clearly the complex bifurcation structures found for $Pe = 5$ (cf. Figure 10) are an intermediate stage between the CSTR ($Pe = 0$, Figure 9) and tubular reactors with large Peclet numbers. Ultimately, we know the plug flow model (which results for $Pe \to \infty$) has neither multiplicity nor oscillations. Thus our calculations in Figures 14, 15 indicate that the S and M lines shown in Figure 10 should move to higher and higher values of (B,β) as the Peclet number increases, and ultimately disappear as $Pe \to \infty$.

Effect of Lewis Number

As mentioned in the introduction, the Lewis number has practical interest in revealing whether or not limit cycles are possible in fixed bed reactors. The Hopf bifurcation analysis provides a means for such a study, and we use it,

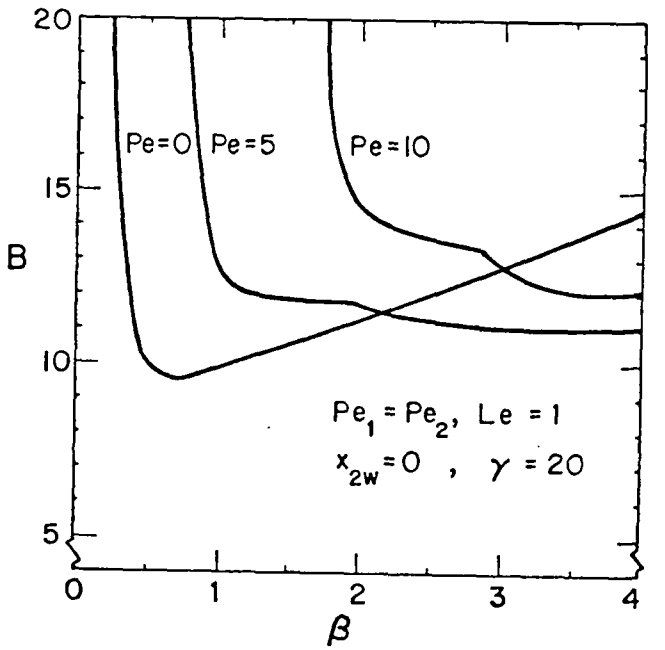

Figure 15 The lower limit for Hopf bifurcation at different values of the Peclet number.

as did Ray and Hastings [67], to determine the critical value of the Lewis number, Le_c, above which oscillations do not occur. Because of the analogy to the CSTR case, one expects oscillations to exist for all $0 < Le < Le_c$, and in fact, extensive numerical calculations support this conjecture.

The bifurcation analysis may be carried through with respect to Le just as was done in the previous sections with respect to Da. In the CSTR case the model parameters can be redefined such that the parameter space plots for $Le = 1$ can be used directly for all values of Le [67]. Unfortunately, in the tubular reactor case, a similar redefinition of the parameters cannot be made because of the convection terms in the modelling equations.

When $N = 1$ in the collocation or Galerkin approximation, it is possible to derive an expression for the Lewis number from the Hopf condition, Eqn. (62a):

$$S_1 = \mathrm{tr}(\underset{\sim}{J}) = \mathrm{tr}(\underset{\sim}{M}_1 + \underset{\sim}{K}_{11}) = 0 \tag{69}$$

By inserting the expressions for $\underset{\sim}{M}_1$ and $\underset{\sim}{K}_{11}$ (25,26) and (30,31) and rearranging, we obtain (for the Galerkin procedure) the expression

$$Le_c = -\frac{\int_0^1 \left.\frac{\partial f_2}{\partial x_2}\right|_s \phi_{21}^2 dz - [\frac{\lambda_{21}}{Pe_2} + \frac{Pe_2}{4} + \beta]}{\int_0^1 \left.\frac{\partial f_1}{\partial x_1}\right|_s \phi_{11}^2 dz - [\frac{\lambda_{11}}{Pe_1} + \frac{Pe_1}{4}]} \tag{70}$$

while for the collocation procedure we have

$$Le_c = -\frac{\left.\frac{\partial f_2}{\partial x_2}\right|_{x_s(z_i)} + \frac{B^*_{211}}{Pe_2} - A^*_{211} - \beta}{\left.\frac{\partial f_1}{\partial x_1}\right|_{x_s(z_i)} + \frac{B^*_{111}}{Pe_1} - A^*_{111}} \tag{71}$$

where both formulae are subject to the constraint $\mathrm{Det}(\underset{\sim}{J}) > 0$.

When $N = 2$, the Hopf condition (63a) may be rearranged to a fourth order polynomial in Le_c by using the fact that the Lewis number divides all elements in the even numbered rows of the Jacobian Equation (17) [37]. However, when $N > 2$, the Hopf bifurcation condition becomes too complex to be expressed in terms of Le_c, and Le_c is then determined iteratively by calculating the eigenvalues of the Jacobian.

In the following paragraphs we give examples of the changes in the bifurcation structure as $Le \to 0$. Figures 16, 17, and 18 show the variation in the critical Lewis number with the Damköhler number in three different cases of steady state behavior, and Table 3 summarizes the corresponding bifurcation regions. In these calculations $N = 6$ terms were used to insure accurate values.

In the first case (Figure 16), the tubular reactor equations have a unique solution for all values of Da. This is globally stable when $Le > Le_c^*$ where

$$Le_c^* = \max_{Da>0} Le_c \, . \tag{72}$$

Table 3 Types of bifurcation behavior for different Pe as Le → 0

($B = 15$, $Pe_1 = Pe_2$, $x_{2w} = 0$, $\beta = 3$, $\gamma = 10$)

Figure	Pe	Le	Regions[+]
16	3	Le>1.39	I
		1.267<Le<1.39	V
		1.262<Le<1.267	XV*
		0 <Le<1.262	V
		1.27 <Le<1.31	III
17	4	1.26 <Le<1.27	IV
		1.22 <Le<1.26	XVI**
		0 <Le<1.22	IV
		Le>1.28	VIIIa
		1.27 <Le<1.28	XI
		1.25 <Le<1.27	IX
18	5	1.22 <Le<1.25	XI
		1.20 <Le<1.22	XIII
		0.844<Le<1.20	X
		0 <Le<0.844	XIV***

+ cf. Figures 10 and 12

* New region, cf. Figure 19b

** New region, cf. Figure 19c

*** cf. Figure 19a

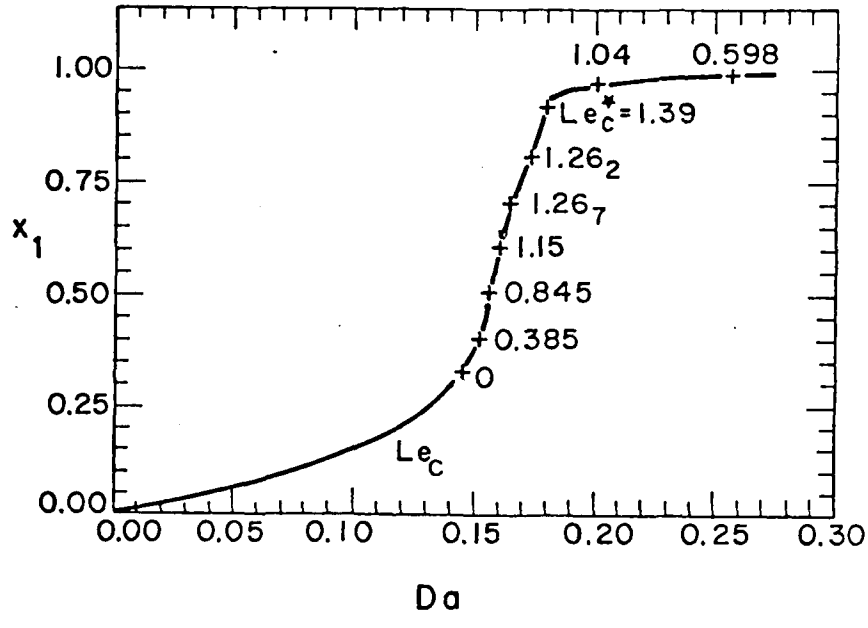

Figure 16 The critical Lewis number, Le_c, and the steady state exit conversion, x_1, for varying Damköhler number, Da. $B = 15$, $Pe_1 = Pe_2 = 3$, $x_{2w} = 0$, $\beta = 3$, $\gamma = 20$.

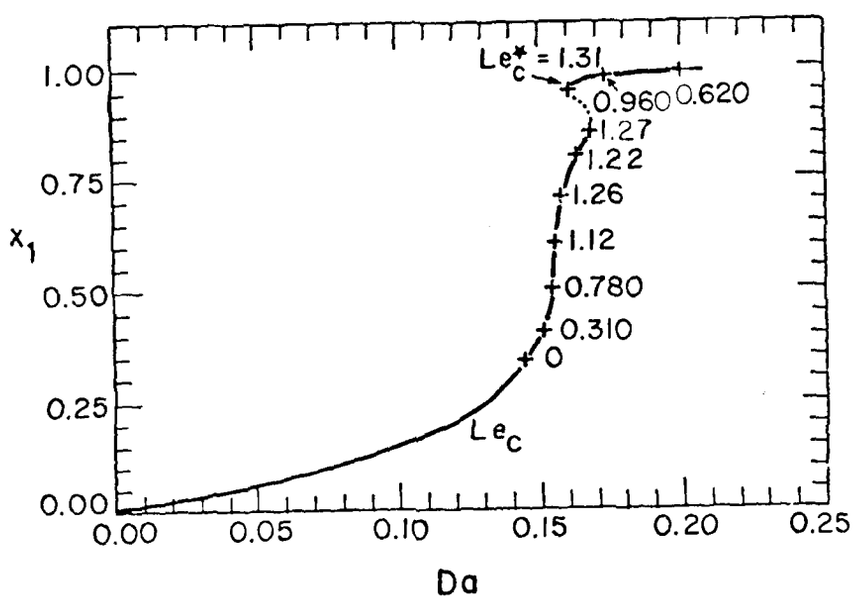

Figure 17 The critical Lewis number, Le_c, and the steady state exit conversion, x_1, for varying Damköhler number, Da. $B = 15$, $Pe_1 = Pe_2 = 4$, $x_{2w} = 0$, $\beta = 3$, $\gamma = 20$.

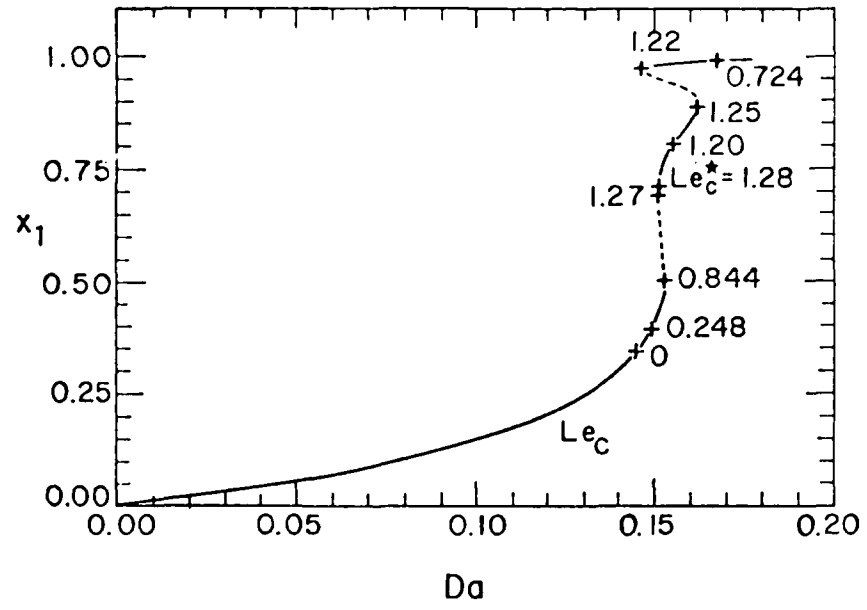

Figure 18 The critical Lewis number, Le_c, and the steady state exit conversion, x_1, for varying Damköhler number, Da. $B = 15$, $Pe_1 = Pe_2 = 5$, $x_{2w} = 0$, $\beta = 3$, $\gamma = 20$.

At $Le_c = 1.39$ a set of Hopf bifurcation points, s_3 and s_4, appears and these move apart as Le decreases. This behavior corresponds to region V. Since Le_c has a second local maximum, $Le_c = 1.267$ at $x_1 = 0.72$, a second set of Hopf points s_1 and s_2 emerges when $Le_c = 1.267$. Thus, there are two intervals of Da numbers where stable oscillations exist. This structure, which was not found above, is classified as region XV and is illustrated by Figure 19b. When $Le = 1.262$ the Hopf points, s_2 and s_3, coalesce and disappear. Thus, we are back in region V.

In the second case (Figure 17), three steady state profiles exist for $0.160 < Da < 0.168$. As Le decreases beneath Le_c^* a Hopf point appears on the upper branch and we have a region III behavior. At $Le = 1.27$ a Hopf point comes onto the lower branch at the turning point and we are then in region IV. Because Le_c versus Da has a local maximum, $Le_c = 1.26$ at $x_1 = 0.71$ and a local minimum, $Le_c = 1.22$ at $x_1 = 0.81$, a second set of Hopf points emerge on the lower branch when $1.22 \leq Le \leq 1.26$. Thus, there are now three bifurcation points on the lower branch plus one on the upper branch. This structure is new and is classified as region XVI. It is illustrated by Figure 19c. For $Le_c < 1.22$ the set of points disappear again and we are back in region IV.

In the third case (Figure 18), we have multiplicity of the kind 1-3-5-3-1. Since Le_c^* is located on the middle branch, we pass from region VIII to XI as Le decreases beneath Le_c^*. At $Le = 1.27$ the Hopf point "falls off" the second turning point and then we have region IX behavior. At $Le = 1.25$ a new

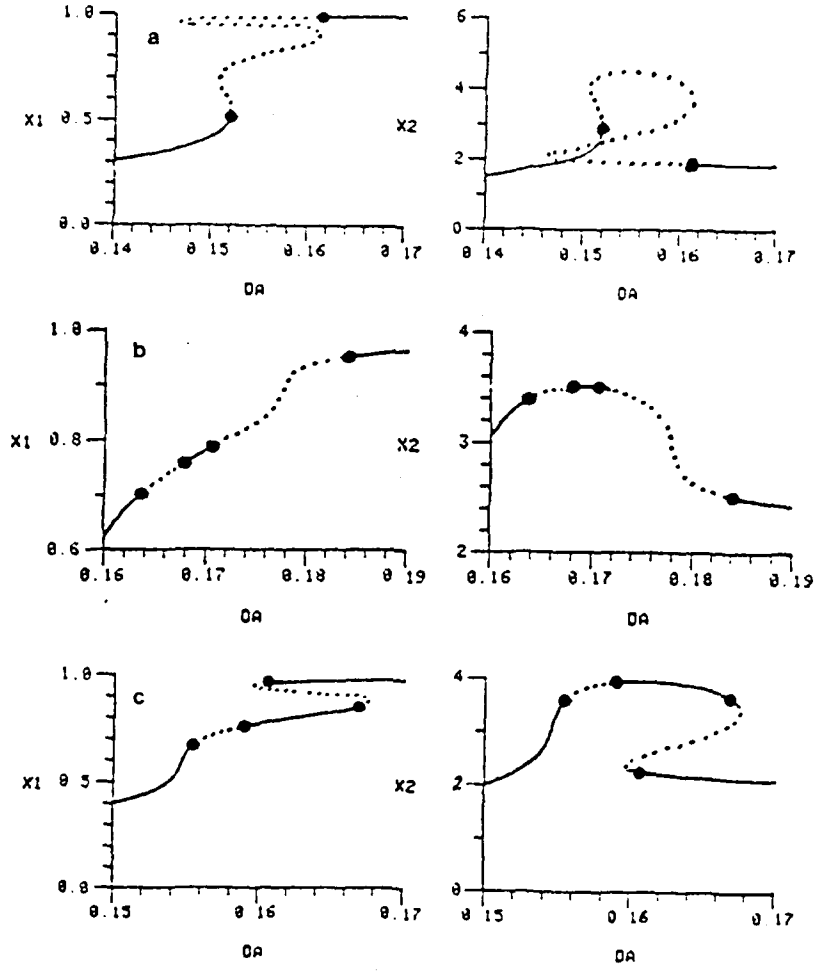

Figure 19 The steady state exit conversion, x_1, and temperature, x_2, for varying Da: B = 15, x_{2_c} = 0.[illegible] = 3, γ = 20.
(a) Example of region XIV behavior: Le = 0.800, $Pe_1 = Pe_2 = 5$
(b) Example of region XV behavior; Le = 1.263, $Pe_1 = Pe_2 = 3$
(c) Example of region XVI behavior; Le = 1.240, $Pe_1 = Pe_2 = 4$

bifurcation point emerges from behind the third turning point and we are back in region XI. When $Le = 1.22$ a Hopf point appears on the upper branch giving us region XIIIa behavior. At $Le = 1.20$ the Hopf points on the middle of the branch coalesce and we have a region Xa structure until $Le_c = 0.844$ where a point emerges on the lower branch (region XIV). This is illustrated by Figure 19a, which indicates the existence of a stable limit cycle surrounding five unstable steady states for a small range of Da just to the right of the lower Hopf bifurcation point.

It is possible to answer the question of existence of limit cycles in fixed bed reactors, by considering the variation in Le_c^* with Pe as illustrated in Figure 20. Here also the influence of the number of terms in the Galerkin expansion is shown. The discontinuities in the curves occur when Le_c^* shifts among branches in the region of multiplicity as is illustrated by Figures 16, 17 and 18. Note that Le_c^* becomes less than unity for $Pe > 14$, which implies that, even for "empty" tubular reactors ($Le = 1$), oscillations are only possible in very short reactors (as was shown in the previous section). Therefore, oscillations due to interaction of mixing and reaction terms should not occur in industrial fixed bed reactors where $Le \sim 500$ are common.

8. CONCLUDING REMARKS

In this paper we have given a detailed analysis of the occurrence of multiple steady states and oscillatory behavior in tubular reactors using the pseudohomogeneous axial dispersion model as an example. This model was a convenient choice since the modelling equations formed a relatively simple

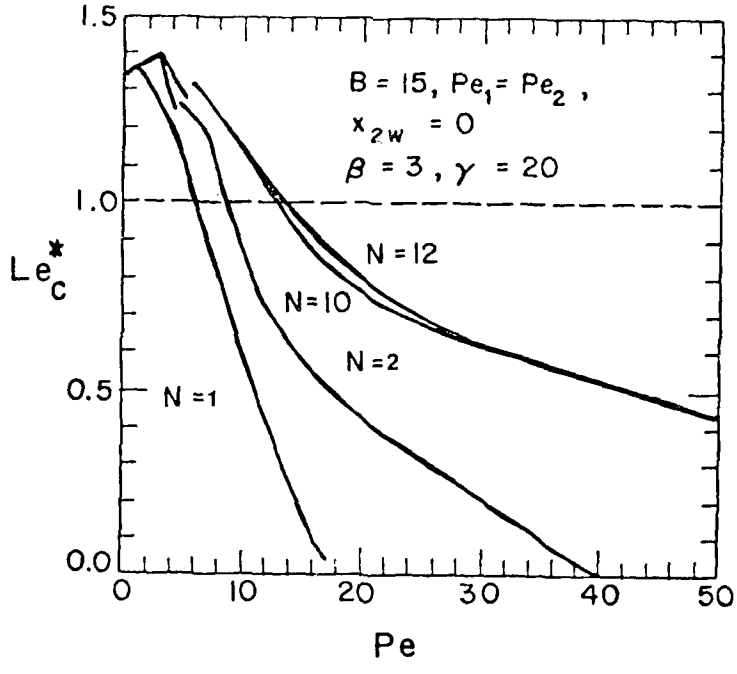

Figure 20 The critical Lewis number, Le_c^*, as a function of the Peclet number, Pe for different number of terms, N, in the Galerkin expansion.

set of nonlinear coupled parabolic partial differential equations. Moreover, previously published examples of multiple steady states and limit cycles for this model made it possible to check the algorithms. Special considerations were given to the solution of stiff steady state equations and, among different approximation procedures, orthogonal spline collocation was found to give the best accuracy. Comparisons of various ways of calculating bifurcation to multiple steady states showed direct turning point calculations to be most convenient. The eigenvalues of the linearized operator were determined by both a collocation and Galerkin procedure. The former converged in a dampened oscillatory manner, while the latter appeared to converge faster and monotonically.

The bifurcation algorithms were sensitive to the accuracy of the steady state calculations so even for moderate Peclet numbers ($Pe \sim 5$) it was necessary to use spline intervals with 6-10 collocation points in each interval. Although orthogonal spline collocation was very efficient in the steady state calculations, this meant that 10-60 minutes of CPU were required on a PDP 11/55 minicomputer in order to trace out the bifurcation behavior for all values of $Da > 0$ when all other parameters were fixed. The actual length of the computations depended on the narrowness of the search interval and the values of B and Pe. To fully describe the types of dynamic behavior possible, one still has to determine the stability and direction of the branching of periodic solutions. This can easily be done within the framework of the present

numerical techniques either by applying standard GLE formulae [79,95,98] to the Galerkin approximation or by using the GLE formulae of Heinemann and Poore [99].

Although in the present study the analysis was focused on a tubular reactor, the algorithms developed here should be useful in determining the bifurcation structures present in other systems described by PDE's. Considering the rich variety of bifurcation structures in the relatively simple axial dispersion tubular reactor model, one can envision the intricate and challenging structures possible in the more complex models.

Acknowledgements:

This work was supported in part by the United States Army under Contract Number DAAG29-80-C-0041 and The National Science Foundation under Grant No. CPE79-21511. Also support in part by the donors of the Petroleum Research Fund administered by the American Chemical Society is gratefully acknowledged.

NOMENCLATURE

A_{kl}	coefficient in Galerkin expansion, defined in Eq. (19)
$A_{k,l}$	collocation weight, see Eq. (27)
B	dimensionless adiabatic temperature rise, defined in Eq. (6)
$B_{k,l}$	collocation weight, see Eq. (28)
B_i	boundary operator, defined in Eq. (11)
C	concentration
C_f	feed concentration
C_{pf}	heat capacity of fluid phase
C_{ps}	heat capacity of solid phase
C	capacitance matrix, defined in Eq. (8)
D_r	diameter of reactor
Da	Damköhler number, defined in Eq. (6)
D_L	longitudinal dispersion coefficient
E_A	activation energy
$f(x)$	nonlinear multivariable function, defined in Eq. (10)
F_x	linear operator, defined in Eq. (16)
ΔH	enthalpy of reaction
J	Jacobian, defined in Eq. (17)
k	pre-exponential factor
k_L	longitudinal thermal conduction
K	2 x 2 matrix, defined in Eqs. (26) and (31)
L	reactor length
L	number of spline points
L	L operator, defined in Eq. (9)
$L_{k,l}$	combined collocation weight, see Eq. (43)
Le	Lewis number, defined in Eq. (6)
Le^*	critical Lewis number

M	number of interior collocation points in steady state solution
$\underset{\sim}{M}_i$	2 x 2 matrix, defined in Eqs. (25) and (30)
N	number of terms in collocation or Galerkin approximation
$\underset{\sim}{p}$	vector of parameter values
$P(\lambda)$	characteristic polynomial, Eq. (58)
Pe_1	Peclet number for mass dispersion, defined in Eq. (6)
Pe_2	Peclet number for heat dispersion, defined in Eq. (6)
R	universal gas constant
s_i	i'th Hopf bifurcation point
S_i	sum of i'th principal minor of Jacobian
t'	time
t	dimensionless time, defined in Eq. (6)
T	temperature
T_w	wall temperature
T_0	feed temperature
U_w	heat transfer coefficient
v_z	linear gas velocity
$\underset{\sim}{x}$	state vector
x_1	conversion, defined in Eq. (6)
x_2	dimensionless temperature, defined in Eq. (6)
x_{2s}	value of x_2 at the spline point, z_s, see Eq. (36)
x_{2w}	dimensionless wall temperature
$\underset{\sim}{y}$	state vector
z'	longitudinal coordinate
z	dimensionless longitudinal coordinate, defined in Eq. (6)
z_i	i'th spline point
z_s	spline point separating the reaction zone from the "dead" zone, see Eq. (36)

Greek Symbols

α_1, α_2	coefficients, defined in Eq. (38)
β	dimensionless heat transfer coefficient, defined in Eq. (6)
γ	dimensionless activation energy, defined in Eq. (6)
δ_{ij}	Kronecker's delta
ε_p	bed porosity
ζ	dimensionless longitudinal coordinate
λ_{kn}	n'th eigenvalue, given in Eq. (23)
μ_i	coefficients, see Eqs. (66) and (67)
ρ_f	density fluid phase
ρ_s	density solid phase
$\phi_{kn}(z)$	n'th eigenfunction, see Eq. (22)
ω	frequency of the bifurcating orbit

[1] Froment, G.F., Chemie Ing. Tech. 1974 46 374.

[2] Amundson, N.R., Berichte Bunsen-Gesel. 1970 74 96.

[3] Froment, G.F., Proc. 2nd Int. Symp. Chem. React. Engng., Elsevier, Amsterdam, 1972, pp. A7-1.

[4] Karanth, N.G. and Hughes, R., Int. Rev.-Sci. Engng. 1974 9 169.

[5] Hlaváček, V. and Votruba, J., in Chemical Reactor Theory, eds. Amundson, N.R. and Lapidus, L., Prentice Hall, New Jersey, 1977, pp. 314.

[6] Hlaváček, V., Can. J. Chem. Engng. 1970 48 656.

[7] Ray, W.H., Proc. 2nd Int. Symp. Chem. React. Engng., Elsevier, Amsterdam, 1972, pp. A8-1.

[8] Wicke, E., Chemie Ing. Tech. 1974 46 365.

[9] Schmitz, R.A., Adv. Chem. Ser. 1975 148 156.

[10] Gilles, E.D., Proc. 4th Int. Symp. Chem. React. Engng., Heidelberg, Dechema, 1976, pp. 499.

[11] Varma, A., and Aris, R., in Chemical Reactor Theory, eds. Amundson, N.R. and Lapidus, L., Prentice Hall, New Jersey, 1977, pp. 79.

[12] Hlaváček, V., and Votruba, J., Adv. Catal. 1978 27 59.

[13] Volter, B.V., Proc. IFAC Congress, 1964, Butterworth, London, pp. 209.

[14] Padberg, G. and Wicke, E., (a) Chem. Engng. Sci. 1967 22 1035. (b) Chemie Ing. Tech. 1969 40 1033.

[15] Wicke, E., Padberg, G. and Arens, H., Proc. 4th Eur. Symp. React. Engng., Brussels, Pergamon Press, 1968, pp. 425.

[16] Root, R.B. and Schmitz, R.A., (a) AIChE J., 1969 15 670. (b) AIChE J., 1970 16 356.

[17] Fieguth, P. and Wicke, E., Chemie Ing. Tech. 1971 43 604.

[18] Luss, D., and Mendellin, P., Proc. 2nd Int. Symp. React. Engng., Elsevier, Amsterdam, 1972, pp. 34-47.

[19] Butakov, A.A. and Maksimov, E.I., Dokl. Akad. Nauk. SSSR 1973 209 643.

[20] Hlaváček, V., and Votruba, J., (a) Int. J. Chem. Engng. 1974 14 461, (b) Adv. Chem. Ser. 1974 133 545.

[21] Renken, A., Müller, M., and Helmuich, H., Chemie Ing. Tech. 1975 47 1029.

[22] Stephens, A.D., Chem. Engng. Sci. 1975 30 11.

[23] Hlaváček, V., Votruba, J., and Hofmann, H., Chem. Engng. Sci. 1976 31 1210.

[24] Votruba, J., Hlaváček, V., and Sinkule, J., Chem. Engng. Sci. 1976 31 971.

[25] Ampaya, J.A. and Rinker, R.G., Chem. Engng. Sci. (a) 1977 32 1327, (b) 1978 33 703.

[26] Hegedus, L.L., Oh, S.E., and Baron, K., AIChE J., 1977 23 632.

[27] Schlegay, R., Jr., and Shah, Y.T., Chem. Engng. Sci., 1977 32 881.

[28] Butakov, A.A. and Shkadinskii, V.G., Dokl. Akad, Nauk SSSR 1978 238 166.

[29] Oh, S.H., Baron, K., Cavendish, J.C., and Hegedus, L.L., ACS Symp. Ser. 1978 65 461.

[30] Mikus, O., Puszynski, J., and Hlaváček, V., Chem. Engng. Sci. 1979 34 436.

[31] Oh, S.H., Baron, K., Sloan, E.M., and Hegedus, L.L., [illegible] 1979 53 272.

[32] [illegible], and Hughes, R., Chem. Engng. Sci. 1979 34, [illegible] 425.

[33] [illegible], V., Mikus, O., Jira, E., and Pour, V., Chem. [illegible] 1980 35 258.

[34] [illegible] and Vortmeyer, D., Chem. Engng. Sci. 1980

[35] [illegible] and Varma, A. Submitted to AIChE J. 1980.

[36] [illegible] and Hlaváček, V., Chem. Engng. Sci. 1980

[37] [illegible], PhD Thesis University of Wisconsin-Madison,

[38] [illegible], V., and Hofmann, H., Chem. Engng. Sci. 1970 25, [illegible] 187.

[39] [illegible]k, V., and Hofmann, H., Chem. Engng. Sci. 1970 25 [illegible].

[40] [illegible], V., Hofmann, H., and Kubíček, M., Chem. Engng. Sci. 1971 [illegible].

[41] Hlaváček, V., Hofmann, H., Votruba, J., and Kubíček, M., Chem. Engng. Sci. 1973 28 1897.

[42] Sinkule, J., Votruba, J., Hlaváček, V., Hofmann, H., Chem. Engng. Sci. 1976 31 23.

[43] Kubíček, M. Hofmann, H., and Hlaváček, V., Chem. Engng. Sci. 1979 34 593.

[44] McGowin, C.R. and Perlmutter, D.D., AIChE J. 1971 17 831.

[45] Varma, A., and Amundson, N.R., Can. J. Chem. Eng. 1973 51, (a) 206, (b) 459.

[46] Kapila, A.K., Poore, A.B., and Heinemann, R.F., submitted to Chem. Eng. Sci.

[47] Vortmeyer, D., Z. Electrochem. 1961 65 282.

[48] Vortmeyer, D., and Jahnel, W., (a) Chemie Ing. Tech. 1971 43 461, (b) Chem. Eng. Sci. 1972 27 1485.

[49] Simon, B., and Vortmeyer, D., Chem. Eng. Sci. 1978 33 109.

[50] Gilles, E.D., Chem. Eng. Sci. 1974 29 1211.

[51] Rhee, H.K., Foley, D., and Amundson, N.R., Chem. Eng. Sci. 1973 28 607.

[52] Rhee, H.K., Lewis, P.P., Amundson, N.R., Ind. Eng. Chem. Fundam. 1974 13 317.

[53] McGowin, C.R., and Perlmutter, D.D., Chem. Eng. J. 1971 2 125.

[54] Georgakis, C., Aris, R., and Amundson, N.R., Chem. Eng. Sci. 1977 32, (a) 1359, (b) 1371, (c) 1381.

[55] Nishimura, Y., and Matsukara, M., Chem. Eng. Sci. 1969 24 1427.

[56] Berger, A.J. and Lapidus, L., AIChE J., (a) 1968 14 356, (b) 1969 15 171.

[57] McGreavey, C., and Soliman, M.A., (a) AIChE J. 1972 19 174, (b) Chem. Eng. Sci. 1973 28 1401.

[58] Varma, A. and Amundson, N.R., (a) Chem. Eng. Sci. 1972 27 907, (b) Can. J. Chem. Eng. 1972 50 470.

[59] Stephanopolous, G., and Schuelke, M.L., AIChE J. 1976 22 855.

[60] Clough, D.E., and Ramirez, W.F., AIChE J. 1972 18 393.

[61] Liou, C. T., Lim, H. C., and Weigand, W.A., (a) AIChE J. 1972 18 875, (b) Chem. Eng. Sci. 1974 29 705.

[82] Byrne, C.D. and Hindmarch, A.C., EPISODE a Polyalgorithm for the Numerical Solution of Ordinary Differential Equations, UCRL-75652, Lawrence Livermore laboratories, California.

[83] Michelsen, M.L., (a) AIChE J. 1976 22 594, (b) Chem. Eng. J. 1977 14 107.

[84] McGinnis, P.H., Jr., Chem. Eng. Prog. Symp. Ser. 1965 55 (61) 2.

[85] Kubíček, M. and Hlaváček, V., Chem. Eng. Sci. 1971 26 321.

[86] Guertin, E.W., Sørensen, J.P., and Stewart, W.E., Computers Chem. Eng. 1977 1 197.

[87] Carey, G.F., and Finlayson, B.A., Chem. Eng. Sci. 1974 30 587.

[88] Birnbaum, I., and Lapidus, L., Chem. Eng. Sci. 1978 33 443.

[89] Lübeck, B., Chem. Engng. J. 1974 7 29.

[90] Keller, H.B., in [71] pp. 359.

[91] Sørensen, J.B., Guertin, E.W., and Stewart, W.E., AIChE J. 1973 969, 1286.

[92] Luss, D., and Amundson, N.R., Can. J. Chem. Engng. 1967 45 341.

[93] Kubíček, M., and Hlaváček, V., Chem. Eng. Sci. 1974 29 1695.

[94] Francis, J.G.F., The Computer Journal, (a) 1961 4 265, (b) 1962 4 332.

[95] Hassard, B., Information Linkage between Applied Mathematics and Industry, Academic Press, 1979 pp. 313.

[96] Gantmacher, F.R., Matrix Theory, Vol. 1, Chelsea Publishing, New York, 1959.

[97] Kubíček, M., (a) Chem. Eng. Sci. 1979 34 1078, (b) SIAM J. Appl. Math. 1980 38 103.

[98] Poore, A.B., Arch. Rational Mech. Anal. 1976 60 371.

[99] Poore, A.B., and Heinemann, R.F., AIChE Annual Meeting, Chicago 1980.

[62] Aronson, D.G., [illegible] 1965 44 [illegible].

[63] Gel'fand, I.M., and Shilov, G.E., Theory Prob. Appl., 1964 24 1141.

[64] Cohen, D.S., in Nonlinear Problems in the Physical Sciences and Biology, Springer Verlag, Berlin, 1973.

[65] Cohen, D.S., and Keller, H.B., SIAM J. Appl. Math. 1974 27 416.

[66] Uppal, A., Ray, W.H., and Poore, A.B., Chem. Eng. Sci., (a) 1974 29 967, (b) 1976 31 205.

[67] Ray, W. H., and Hastings, S., Chem. Eng. Sci. 1980 35 549.

[68] Sattinger, D.H., Topics in Stability and Bifurcation Theory, Springer Verlag, Heidelberg 1973.

[69] Keller, J.B., in Bifurcation Theory and Nonlinear Eigenvalue Problems, eds. Keller, J.B. and Artman, S., W.A. Benjamin, New York 1969.

[70] Marsden, J.E. and McCracken, M., The Hopf Bifurcation Theory and its Applications, Springer Verlag, New York 1976.

[71] Rabinowitz, P.H. (ed.), Applications of Bifurcation Theory, Academic Press, New York 1977.

[72] Crandall, M.G. and Rabinowitz, P.H., Arch. Rational Mech. Anal. 1973 52 161.

[73] Crandall, M.G. and Rabinowitz, P.H., in Dynamical Systems, Academic Press, New York 1977 pp. 27.

[74] Crandall, M.G. and Rabinowitz, P.H., Arch. Rational Mech. Anal. 1978 67 53.

[75] Crandall, M.G., in [71] pp. 1.

[76] Finlayson, B.A., SIAM J. Numer. Anal. 1971 8 316.

[77] Finlayson, B.A., The Method of Weighted Residuals and Variational Principles, Academic Press, New York 1972.

[78] Villadsen, J. and Stewart, W.E., Chem. Eng. Sci. 1967 22 1483.

[79] Villadsen, J., Selected Approximation Methods for Chemical Engineering Problems, Instituttet for Kemiteknik, DtH, Lyngby, Denmark 1970.

[80] Finlayson, B.A., Cat. Rev.-Sci. Eng. 1974 10 69.

[81] Michelsen, M.L., and Villadsen, J., Solution of Differential Equation Models by Polynomial Approximation, Prentice Hall, New Jersey 1978.

Figure 1 Behavior of the interpolating polynomial (a) compared to the exact solution (b). Approximate solution based on orthogonal collocation, M = 10. Reactor parameters: B = 10.0, Da = 0.13, Pe_1 = Pe_2 = 1[illegible], β = 0.0, γ = 20.0.

Figure 2 Steady state bifurcation curves based on steady state solutions with orthogonal collocation (A) and spline collocation (M = 10) (B); B = 10.0, β = 0.0, γ = 2[illegible].

Figure 3 Example of a steady state profile for which three spline points (●) are necessary. B = 16.8, Da = 0.337, Pe_1 = 320, Pe_2 = 100, x_{2w} = -9.6, β = 0.72, γ = 16.9.

Figure 4 An example of steep conversion and temperature profiles found by spline collocation. (a) Upper steady state, (b) lower steady state. B = 16.8, Da = 0.330, Pe_1 = 320, Pe_2 = 100, x_{2w} = 9.6, β = 0.72, γ = 16.9.

Figure 5 Ignition and extinction behavior of outlet conversion and temperature for Lübeck's example [89]. Pe_1 = 3[illegible], Pe_2 = 100, β = 0.72, B = $8.7 \cdot 10^6 T_f^{-2}$, Da = $7.33 \cdot 1[illegible] T_f^{-9}$, γ = $1.22\ 10^4 T_f^{-1}$, x_{2w} = $\gamma(310-T)T_f^{-1}$, T_f feed temperature in °K.

Figure 6 Steady state value of $x_1(z)$ for varying Da. The curve has two turning points, m_1 and m_2.

Figure 7 The predicted bifurcation points, Da_b, for various assumed values, Da_s, and varying number of terms, N, in the Galerkin expansion.

Figure 8 The critical Lewis number, Le_c^*, for varying number of terms, N, in the collocation procedure (x) and in Galerkin's method (o).

Figure 9 Classification of the dynamic behavior of the CSTR in the parameter space B-β [66].

Figure 10 Classification of the dynamic behavior of the axial dispersion model (Pe = 5) in the parameter space B-β. In the peripheral figures: —— stable state, ---- unstable state, ● Hopf bifurcation points.

Figure 11 Classification of the dynamic behavior of the axial dispersion model (Pe = 5) in the parameter space B-β. Cf. Figure 12a-r and Table 2 for further details.

Figure 13 The steady state exit conversion, x_1, and temperature, x_2, for various Da.
— = stable state, --- = unstable state,
• = Hopf bifurcation point. (Cf. Table 2 for parameters.)

Figure 14 Steady state profiles; — = stable, --- unstable
(i) case b Table 5 (Region II); Da = 0.136
(ii) case i Table 5 (Region IV); Da = 0.185
(iii) case j Table 5 (Region XIIIb); Da = 0.144
(iv) case k Table 5 (Region XIIIt); Da = 0.156
v) case l Table 5 (Region VIII); Da = 0.070

Figure 15 Comparison of exact and approximate limits of multiplicity.

Figure 16 The lower limit for Hopf bifurcation at different values of the Peclet number.

Figure 17 The critical Lewis number, Le_c, and the steady state exit conversion, x_1, for varying Damköhler number, Da. $B = 15$, $Pe_1 = Pe_2 = 3$, $x_{2w} = 0$, $\beta = 3$, $\gamma = 20$.

Figure 18 The critical Lewis number, Le_c, and the steady state exit conversion, x_1, for varying Damköhler number, Da. $B = 15$, $Pe_1 = Pe_2 = 4$, $x_{2w} = 0$, $\beta = 3$, $\gamma = 20$.

Figure 19 The critical Lewis number, Le_c, and the steady state exit conversion, x_1, for varying Damköhler number, Da. $B = 15$, $Pe_1 = Pe_2 = 5$, $x_{2w} = 0$, $\beta = 3$, $\gamma = 20$.

Figure 20 The steady state exit conversion, x_1, and temperature, x_2, for varying Da: $B = 15$, $x_{2w} = 0$, $\beta = 3$, $\gamma = 20$.
(a) Example of region XIV behavior; Le = 0.800, $Pe_1 = Pe_2 = 5$
(b) Example of region XV behavior; Le = 1.263, $Pe_1 = Pe_2 = 3$
(c) Example of region XVI behavior; Le = 1.240, $Pe_1 = Pe_2 = 4$

Figure 21 The critical Lewis number, Le_c^*, as a function of the Peclet number, Pe for different number of terms, N, in the Galerkin expansion.

SECURITY CLASSIFICATION OF THIS PAGE (When Data Entered)

REPORT DOCUMENTATION PAGE

1. REPORT NUMBER: 2172 14 MRC-T-1-2	2. GOVT ACCESSION NO. AD-A099360
4. TITLE (and Subtitle): THE BIFURCATION BEHAVIOR OF TUBULAR REACTORS	5. TYPE OF REPORT & PERIOD COVERED: Summary Report - no specific reporting period
7. AUTHOR(S): Klavs F. Jensen and W. Harmon Ray	8. CONTRACT OR GRANT NUMBER(S): DAAG29-80-C-0041 NSF-CPE79-21512
9. PERFORMING ORGANIZATION NAME AND ADDRESS: Mathematics Research Center, University of Wisconsin 610 Walnut Street Madison, Wisconsin 53706	10. PROGRAM ELEMENT, PROJECT, TASK AREA & WORK UNIT NUMBERS: 2 - Physical Mathematics
11. CONTROLLING OFFICE NAME AND ADDRESS: (See Item 18 below)	12. REPORT DATE: January 1981
	13. NUMBER OF PAGES: 87
14. MONITORING AGENCY NAME & ADDRESS(if different from Controlling Office)	15. SECURITY CLASS (of this report): UNCLASSIFIED
	15a. DECLASSIFICATION/DOWNGRADING SCHEDULE

16. DISTRIBUTION STATEMENT (of this Report)

Approved for public release; distribution unlimited.

17. DISTRIBUTION STATEMENT (of the abstract entered in Block 20, if different from Report)

18. SUPPLEMENTARY NOTES

U. S. Army Research Office
P.O. Box 12211
Research Triangle Park
North Carolina 27709

National Science Foundation
Washington, D. C. 20550

19. KEY WORDS (Continue on reverse side if necessary and identify by block number)

Bifurcation, partial differential equations, chemical reactors, computational methods

20. ABSTRACT (Continue on reverse side if necessary and identify by block number)

Methods for studying the bifurcation behavior of tubular reactors have been developed. This involves the application of static and Hopf bifurcation theory for PDE's and the very precise determination of steady state profiles. Practical computational methods for carrying out this analysis are discussed in some detail. For the special case of a first order, irreversible reaction in a tubular reactor with axial dispersion, the bifurcation behavior is classified and summarized in parameter space plots. In particular the influence of the Lewis and Peclet numbers is investigated. It is shown that

DD FORM 1 JAN 73 1473 EDITION OF 1 NOV 65 IS OBSOLETE

UNCLASSIFIED

SECURITY CLASSIFICATION OF THIS PAGE (When Data Entered)

oscillations due to interaction of dispersion and reaction effects should not exist in fixed bed reactors and moreover, should only occur in very short "packed" tubular reactors. The parameter study not only brings together previously published examples of multiple and periodic solutions but also reveals a hitherto undiscovered wealth of bifurcation structures. Sixteen of these structures, which come about by combinations of as many as four bifurcations to multiple steady states and four bifurcations to periodic solutions, are illustrated with numerical examples. Although the analysis is based on the pseudohomogeneous axial dispersion model, it can readily be applied to other reaction diffusion equations such as the general two phase model for fixed bed reactors.

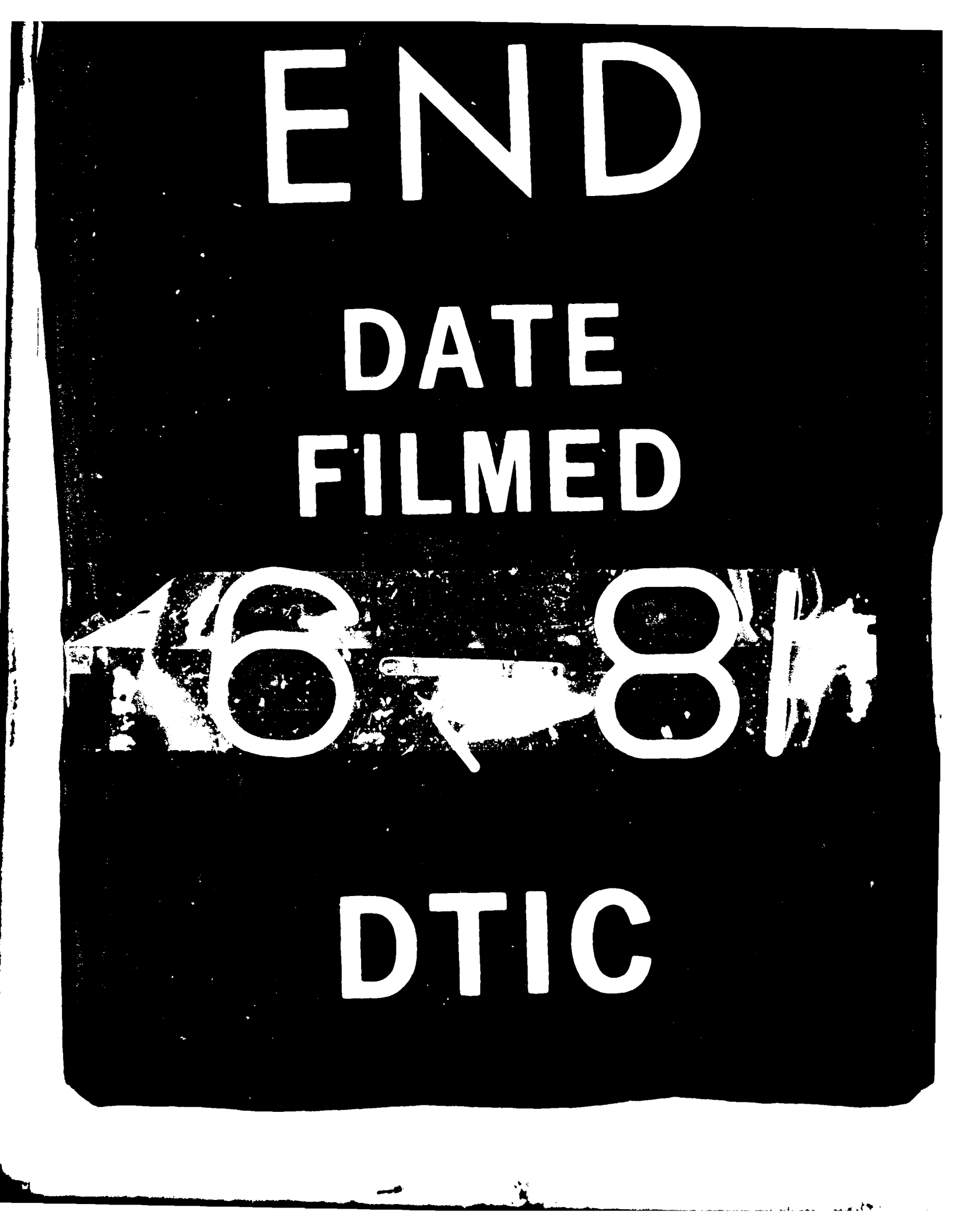
END
DATE
FILMED
6-8
DTIC